Engineering Journal

American institute of steel Construction

first Quarter 2014 Volume 51, No. 1

www.aisc.org

ENGINEERING JOURNAL

AMERICAN INSTITUTE OF STEEL CONSTRUCTION

Dedicated to the development and improvement of steel construction, through the interchange of ideas, experiences and data.

Editorial staff

Editor: Keith A. Grubb, S.E., P.E.
Research Editor: Reidar Bjorhovde, Ph.D.
Production Editor: Areti Carter

off icers

Jeffrey E. Dave, P.E., *Chairman*
Dave Steel Company, Inc., Asheville, NC

James G. Thompson, *Vice Chairman*
Palmer Steel Supplies, Inc., McAllen, TX

Roger E. Ferch, P.E., *President*
American Institute of Steel Construction, Chicago

David B. Ratterman, *Secretary & General Counsel*
American Institute of Steel Construction, Chicago

Charles J. Carter, S.E., P.E., Ph.D., *Vice President and Chief Structural Engineer*
American Institute of Steel Construction, Chicago

Jacques Cattan, *Vice President*
American Institute of Steel Construction, Chicago

John P. Cross, P.E., *Vice President*
American Institute of Steel Construction, Chicago

Scott L. Melnick, *Vice President*
American Institute of Steel Construction, Chicago

The articles contained herein are not intended to represent official attitudes, recommendations or policies of the Institute. The Institute is not responsible for any statements made or opinions expressed by contributors to this Journal.

The opinions of the authors herein do not represent an official position of the Institute, and in every case the officially adopted publications of the Institute will control and supersede any suggestions or modifications contained in any articles herein.

The information presented herein is based on recognized engineering principles and is for general information only. While it is believed to be accurate, this information should not be applied to any specific application without competent professional examination and verification by a licensed professional engineer. Anyone making use of this information assumes all liability arising from such use.

Manuscripts are welcomed, but publication cannot be guaranteed. All manuscripts should be submitted in duplicate. Authors do not receive a remuneration. A "Guide for Authors" is printed on the inside back cover.

ENGINEERING JOURNAL (ISSN 0013-8029) is published quarterly. Subscriptions: Members: one subscription, $40 per year, included in dues; Additional Member Subscriptions: $40 per year. Non-Members U.S.: $160 per year. Foreign (Canada and Mexico): Members $80 per year. Non-Members $160 per year. Published by the American Institute of Steel Construction at One East Wacker Drive, Suite 700, Chicago, IL 60601.

Periodicals postage paid at Chicago, IL and additional mailing offices. **Postmaster:** Send address changes to ENGINEERING JOURNAL in care of the American Institute of Steel Construction, One East Wacker Drive, Suite 700, Chicago, IL 60601.

Copyright 2014 by the American Institute of Steel Construction. All rights reserved. No part of this publication may be reproduced without written permission. The AISC logo is a registered trademark of AISC.

Subscribe to *Engineering Journal* by visiting our website **www.aisc.org/ej** or by calling 312.670.5444.

Copies of current and past *Engineering Journal* articles are available free to members online at **www.aisc.org/ej.**

Non-members may purchase *Engineering Journal* article downloads at the AISC Bookstore at **www.aisc.org/ej** for $10 each.

Experimental Investigation of Steel Joist Design for Ductile Strength Limit State

JOSEPH ROBERT YOST, TIMOTHY J. HARRINGTON, JOSEPH J. POTE, SHAWN P. GROSS and DAVID W. DINEHART

ABSTRACT

Open web steel joists are prefabricated truss assemblies designed in accordance with specifications set forth by the Steel Joist Institute (SJI). Currently, the SJI design requirement is based on capacity, with no consideration for the governing-member strength limit state. The purpose of this research is to investigate a ductile design methodology for steel joists where the primary strength limit state is characterized by tension-member yielding and large inelastic deformation, followed by a secondary strength limit state of compression-member buckling. To achieve ductile behavior, a series of experimental joists were designed and manufactured using controlled over-strength ratios of relative member strengths so that tension-member yielding precluded compression-member buckling. The consequence of adjusting member strengths to induce ductile failure is a slight increase in joist weight. The experimental matrix consisted of 18 joist samples: six identical 33-ft-long K-series joists, six identical 33-ft-long LH-series joists and six identical 32-ft-long rod web joists. All joists were tested to collapse under simply supported uniform load conditions. Experimental results show that a ductile design is achievable because all 18 joists demonstrated tension-member yielding with significant deformation prior to a secondary limit state of compression-member buckling.

Keywords: steel joists, strength design, yielding, ductile limit state.

INTRODUCTION

Open web steel joists are prefabricated truss assemblies typically used in supporting roof and floor systems. The current specification for steel joist design is published by the Steel Joist Institute (SJI) and titled *Standard Specifications, Load Tables and Weight Tables for Steel Joists and Joist Girders,* 43rd edition (SJI, 2010). This specification is based on the 2005 AISC *Specification for Structural Steel Buildings*, ANSI/AISC 360-05, and has a dual format allowing either allowable stress design (ASD) or load and resistance factor design (LRFD). The strength limit state for steel joist members occurs by tension yield, compression buckling or interaction between axial force and bending moment. Presently, the SJI acknowledges four main joist types: K-series joists, longspan joists (LH-series), deep longspan joists (DLH-series) and joist girders. This paper explores the LRFD design methodology as related to design and behavior of K-series and LH-series joists.

In accordance with the current SJI design specifications, individual joist members are designed to meet strength requirements for a given design load combination. Using the LRFD design methodology, the member-strength design requirement may be expressed as follows:

$$\left\{ SR = \frac{f_u}{\phi F_n} \right\} \leq 1.0 \qquad (1)$$

In Equation 1, SR is member specific and defined as the stress ratio, f_u is the required strength or member stress resulting from external factored loads and ϕF_n is the design strength at the ultimate limit state. Both f_u and ϕF_n are defined for K-series joists and LH-series joists in Sections 4.2 and 103.2 of the SJI design specification, respectively (SJI, 2010). In effect, the SR is a measure of member efficiency, where $SR = 1.0$ indicates a member at its design capacity and $SR < 1.0$ indicates reserve strength.

Typically, joists are designed for economy so that individual design stress ratios of multiple tension and compression members are all simultaneously at or near 1.0. Therefore, no consideration is given by the SJI standard (2010) to controlling the member-strength capacity limit state, and ductile tensile yielding (of the bottom chord or tension web) is given no specified preference over sudden compressive

Joseph Robert Yost, Associate Professor, Department of Civil and Environmental Engineering, Villanova University, Villanova, PA (corresponding). Email: joseph.yost@villanova.edu

Timothy J. Harrington, Graduate Research Assistant, Department of Civil and Environmental Engineering, Villanova University, Villanova, PA. Email: tharri04@villanova.edu

Joseph J. Pote, Director of Research and Development, New Millennium Building Systems, LLC, Hope, AR. Email: Joe.Pote@newmill.com

Shawn P. Gross, Associate Professor, Department of Civil and Environmental Engineering, Villanova University, Villanova, PA. Email: shawn.gross@villanova.edu

David W. Dinehart, Professor, Department of Civil and Environmental Engineering, Villanova University, Villanova, PA. Email: david.dinehart@villanova.edu

Table 1. Design Conditions and Ductile Design Limits						
	Design Condition		Relative Strength Factor ρ_{max}		Slenderness Limit	
Member	K-Series	LH-Series	Existing	Ductile Design	Existing	Ductile Design
Bottom chord and end web	Axial tension		None	1.00	240	300
Top-chord interior panel less than 24 in.	Axial compression	Interaction		0.90	90	No change
Top-chord interior panel greater than 24 in.	Interaction					
Top-chord end panel					120	
Interior tension web	Axial tension			0.95	240	
Compression web	Axial compression			0.80	200	

buckling (of the top chord or compression web). As well, in truss design for non-seismic-load cases, the 2005 AISC *Specification* does not make specific reference to a preferred member-strength limit state. Importantly, the discussion here neglects connection-related limit states and is restricted to the member-level joist design, where the strength limit state will occur by tension-member yield or compression-member buckling. At the member level, research has shown that buckling of a steel joist compression member results in an instantaneous and significant loss in load bearing capacity (Yost et al., 2004, 2006). The authors suggest that, given this behavior, a joist designed for a ductile tensile-member yield limit state is desired over one with a sudden compression-member buckling limit state. In the event of severe overloads, the gradual yielding and deformation of a ductile element provides visual warning, load sharing to neighboring members and time for evacuation. Additionally, there is inherently less strength variance in components that are controlled by tensile yield limit state than those controlled by compression limit states, where force eccentricity, variability in end fixity and other variables contribute to less predictable buckling strengths. This characteristic was noted by Engelhardt et al. (2000) as related to strength and failure mode of experimental open web steel joists and by Rao et al. (2011) as related to strength and failure of lattice-type transmission towers.

The objective of this research study is experimental investigation of a steel joist design methodology where ductile tensile yielding is the intended primary-strength limit state. As the controlling tension member(s) yield, the load-bearing capacity of the joist remains intact. Ultimately, with sufficient inelastic deformation and in the absence of tensile fracture, the yield limit state is followed by a secondary strength limit state of compression-member buckling. At compression-member buckling, the joist strength is drastically reduced and ultimate collapse occurs. This paper outlines a design philosophy investigated with experimental testing of K-series and LH-series joists that have been designed for a ductile tensile yielding limit state. The focus of the study is exploratory, where experimental results are compared to predicted behavior in terms of load capacity and strength limit state mechanisms. From this comparison, conclusions are established regarding further pursuit of the proposed ductile methodology as related to steel joist design.

EXISTING SJI DESIGN REQUIREMENTS AND METHODOLOGY

Open-web steel joists are designed in accordance with SJI (2010), which has both LRFD and ASD methodologies. Design considerations not explicitly covered by SJI follow the AISC *Specification for Structural Steel Buildings* (AISC, 2005) or the AISI (American Iron and Steel Institute) *North American Specification for the Design of Cold-Formed Steel Structural Members* (AISI, 2007). LRFD is a probability-based philosophy that implements both load and resistance factors to ensure a minimal chance of inadequate capacity due to overload and/or understrength. This paper will focus solely on the LRFD methodology.

For K-series and LH-series joists, bottom chord and web members are designed for axial force only. Also, interior top chord panels of K-series joists that are less than 24 in. in length are designed for axial compression only. All other K-series and LH series top-chord panels must consider axial compression and bending interaction. Table 1 summarizes these design conditions for all members. The SJI (2010) LRFD design requirements for axial tension, axial compression and interaction are given in Equations 2 through 6 as follows:

$$\text{Axial tension:} \qquad \frac{P_u/A_g}{\phi_t F_y} \le 1 \tag{2}$$

Axial compression: $$\frac{P_u/A_g}{\phi_c F_{cr}} \le 1 \quad (3)$$

Interaction at panel point: $$\frac{f_{au}}{\phi_c F_y} + \frac{f_{bu}}{\phi_b F_y} \le 1 \quad (4)$$

Interaction at mid-panel:

$$\text{for } \frac{f_{au}}{\phi F_{cr}} \ge 0.20 \quad \frac{f_{au}}{\phi_c F_{cr}} + \frac{8}{9}\left[\frac{C_m f_{bu}}{\left(1-\frac{f_{au}}{\phi_c F_e}\right) Q\phi_b F_y}\right] \le 1.0 \quad (5)$$

$$\text{for } \frac{f_{au}}{\phi F_{cr}} < 0.20 \quad \frac{f_{au}}{2\phi_c F_{cr}} + \left[\frac{C_m f_{bu}}{\left(1-\frac{f_{au}}{\phi_c F_e}\right) Q\phi_b F_y}\right] \le 1.0 \quad (6)$$

The numerator terms of Equations 2 through 6 are LRFD required strength terms defined as:

P_u = factored axial force
M_u = factored bending moment
A_g = member cross-sectional area
S = minimum section modulus about axis of bending
f_{au} = factored axial compression stress = P_u/A_g
f_{bu} = factored bending stress = M_u/S
C_m = moment factor taken as
= $1 - 0.3f_{au}/\phi_c F_e$ for end panels
= $1 - 0.4f_{au}/\phi_c F_e$ for interior panels
F_e = Euler buckling stress = $\pi^2 E/(kL/r)^2$
F_y = yield stress assumed for design as 50 ksi
kL/r = maximum member slenderness
E = elastic modulus = 29,000 ksi

The denominator terms of Equations 2 through 6 are LRFD design strength terms and, for those not yet defined, are given as follows:

F_{cr} = $Q\left[0.658^{QF_y/F_e}\right]F_y$ for $kL/r \le 4.71\left(E/QF_y\right)^{1/2}$
= $0.877F_e$ for $kL/r > 4.71\left(E/QF_y\right)^{1/2}$
Q = reduction factor for slender compression elements
k = effective length factor
L/r = member slenderness
ϕ_t, ϕ_c, ϕ_b = resistance factors for tension, compression and bending, respectively
= 0.90

The effective length factor (k) is specified by the SJI specification (SJI, 2010) based on the joist series and member type. In addition to the design strength requirement identified in Equations 2 through 6, SJI also limits the maximum slenderness ratio (L/r) for the various member types. A summary of existing SJI design requirements as related to design condition and maximum slenderness is given in Table 1.

DUCTILE DESIGN PARAMETER AND METHODOLOGY

To design an open-web steel joist for a controlling, ductile tensile–yielding, strength limit state, the relative strengths of the individual members must be considered so that tension yielding precedes compression-member buckling. Thus, using the ductile design philosophy, the maximum stress ratio must be controlled by a tension member, and compression-member stress ratios must be sufficiently less to ensure yield before bucking. Accordingly, the relative strength factor (ρ) has been implemented to require minimum over-strength for all compression members (top chord and interior webs), as a function of the maximum member stress ratio. The relative strength relationship is given as:

$$\left\{\rho_i = \frac{(SR)_i}{(SR)_{\max}}\right\} \quad (7)$$

In Equation 7, ρ_i is the member relative strength factor, $(SR)_i$ is the corresponding member stress ratio and $(SR)_{max}$ is the maximum stress ratio for all members. Again, for a ductile design, $(SR)_{max}$ will be controlled by a tension member.

The stress ratios (SR) are as defined in Equation 1 and calculated using the procedures of Equations 2 through 6. Accordingly, as a structural system, the primary strength limit state of the joist will depend on the maximum relative strength factor for the tension and compression member groups. This relationship is shown in Table 2, where it is noted that to achieve a ductile limit state, $\rho < 1.00$ for all compression members and $\rho = 1.00$ for the maximum tension member. It is understood that these ρ limits are theoretical values, and the maximum ρ for all compression members will need to be less than 1.00 by a sufficient amount so that a tension yielding strength limit state is statistically probable. For this paper, the ρ factor is used in member selection and design of experimental joists so that ductile tensile yielding of end web or bottom chord is the primary strength limit state.

With regard to compression member over-strength, the aforementioned relative strength factor (ρ defined in Equation 7) is the primary design variable governing member selection and achievement of a ductile limit state. A ductile design is theoretically achieved by setting the relative strength factor for the compression members to some value less than 1.00, as noted in Table 2. The lower relative strength factor encourages a ductile limit state by providing additional strength to compression members. Statistically,

Table 2. Relative Strength Factor and Limit States			
	Member Group		
Relative Strength Factor	Compression	Tension	Primary Strength Limit State
ρ_{i-max}	< 1.00	= 1.00	Tensile yield
	= 1.00	= 1.00	Simultaneous tensile yield and compression buckling
	= 1.00	< 1.00	Compression buckling

the lower ρ factor on the compression members decreases their probability of failure. The maximum member relative strength factors used for design of experimental K-series, rod-web K-series and LH-series joists tested in this research, defined as ductile designs, are as follows:

- Bottom chord and end web members $\rho_{max} = 1.00$
- Interior tension webs $\rho_{max} = 0.95$
- Compression web members $\rho_{max} = 0.80$
- Top chord $\rho_{max} = 0.90$

The use of these values results in the prediction of bottom-chord or end-web tension yielding as the primary strength limit state, followed by top-chord buckling as the secondary strength limit state. Again, the relative strength factors are determined using Equation 7, with the stress ratios as given in Equation 1, and the selected members satisfy the proposed maximum relative strength limits. As part of the ductile design methodology, the maximum slenderness limit on end-web and bottom-chord tension members is increased from 240 to 300. The slenderness limit of 300 is consistent with the recommended maximum slenderness ratio for tension members in Section D1 of the 2005 AISC *Specification*. The ductile design parameter limits are summarized in Table 1.

From the maximum ρ factors noted, the compression web has the most reserve strength, with $\rho_{max} = 0.80$. The top chord, in comparison, has a smaller margin of relative over-strength, with $\rho_{max} = 0.90$. In selecting these values, it was considered that compression-web buckling is more variable than top-chord buckling, justifying the lower relative strength factor. The web-strength variability is due to the unsupported condition of the member length, variation in end fixity and eccentricity of axial load resulting from weld location and member alignment. In comparison, the top chord is typically continuously braced by the supporting deck, resulting in more predictable behavior. Also, the top chord is a continuous double-angle member, and size selection is generally controlled by the middle-panel stress ratio. For economy of the joist, top-chord selection is critical and excess over-strength is to be avoided. As well, the top-chord compression strength is known to be higher than that predicted using SJI procedures from research done by Iaboni et al. (2007) and Cianci et al. (2009). These results were all considered in setting the compression-web and top-chord ρ_{max} at 0.80 and 0.90, respectively, for design of the experimental joists. Future research may justify different ρ_{max} values for the compression members.

In conclusion, the proposed relative strength factors promote design of a joist with a high probability of tension member yielding and associated ductile limit state. Introducing a design parameter that regulates the respective strengths of compression and tension members resulted in the joist designs tested in this experimental study. Importantly, the ductile design procedure is offered as an exploratory exercise to investigate feasibility of the ductile design philosophy.

SAMPLE DETAILS AND EXPERIMENTAL PROGRAM

Experimental investigation included testing modified versions of three series of joists: K-series, LH-series and rod-web K-series, each designed per the ductile joist design procedure described earlier (and summarized in Table 1). For statistical validation, six identical samples were tested for each joist series. Figure 1 provides experimental load and support information, and Figure 2 provides sample details related to panel point layout and member sizes. The testing apparatus for all 18 joists was designed to simulate a uniformly distributed load on a simply supported span. Referring to Figure 1, the joists are loaded via four hydraulic cylinders, spaced 8 ft apart. The hydraulic load was manually pumped into the system and equally distributed to each of the four cylinders. As shown in detail A of Figure 1, each cylinder contacts a built-up load distribution unit that further distributes the load into eight point loads on the top chord at 1-ft spacing. The system applies 32 equal point loads, spaced at 1 ft on center, along the 32- or 33-ft length of the joist. Accordingly, the distributed force pattern, w, applied to the top chord is calculated as $w = P_{total}/32$ ft. The top chord was laterally braced at 2-ft intervals to prevent out-of-plane buckling. This combines with the multiple-point loads to simulate a uniformly loaded, continuously braced top-chord condition typical for joists. Additionally, the bottom chord

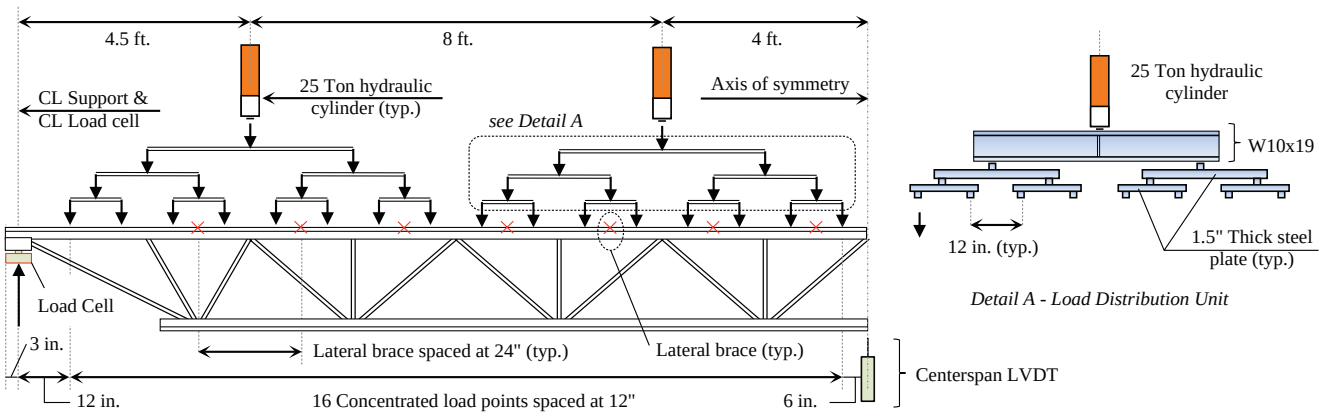

Fig. 1. Experimental load and support detail.

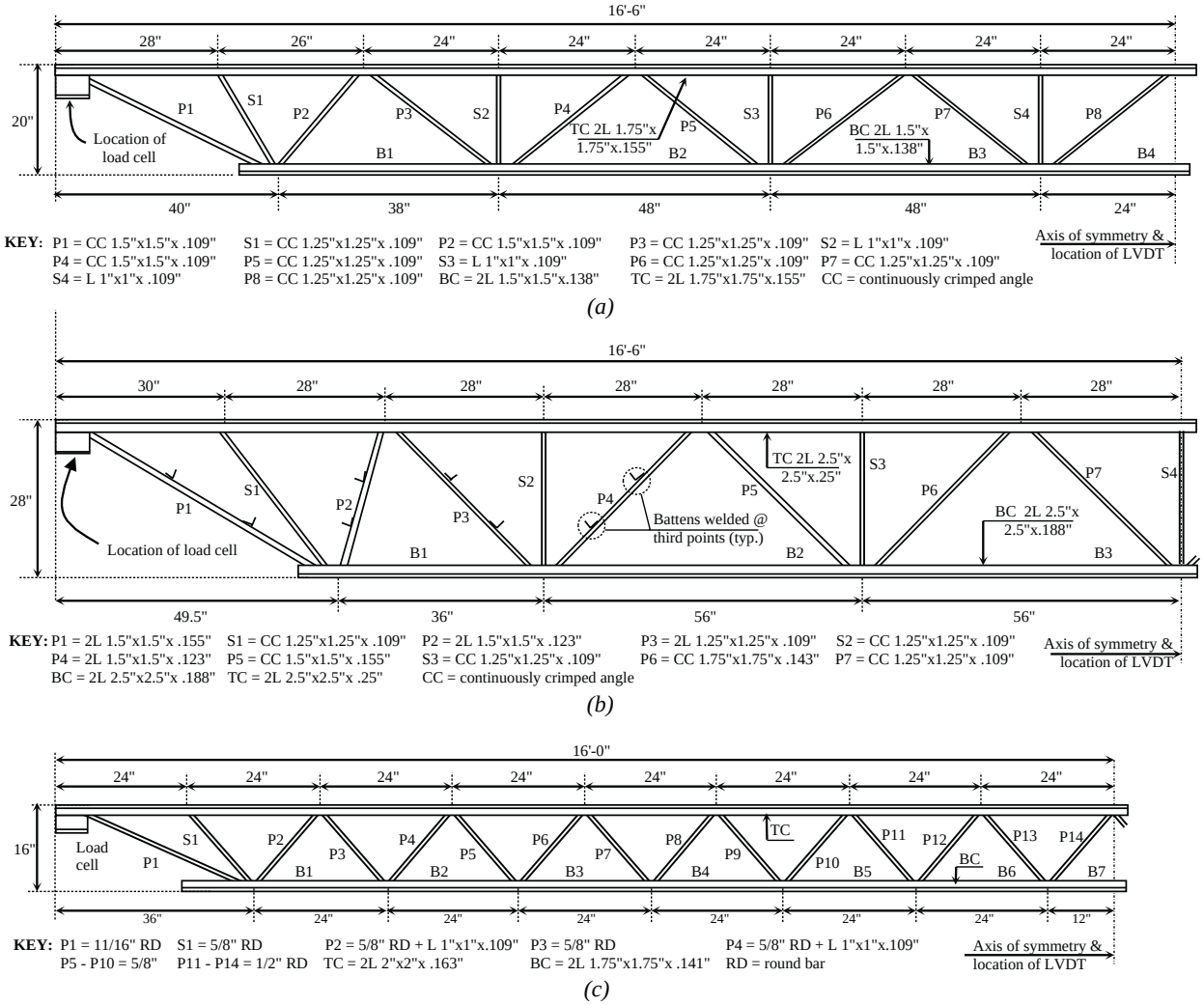

Fig. 2. Sample details: (a) typical K-series details (samples J1-1 through J1-6); (b) typical LH-series details (samples J2-1 through J2-6); (c) typical rod-web K-series details (samples J3-1 through J3-6).

Table 3. Sample Design Parameters and Failure Sequence								
			K-Series		LH-Series		Rod Web	
Member		ρ_{max} (–)	SR and ρ (–)	Predicted Strength Limit State Sequence	SR and ρ (–)	Strength Limit Sequence	SR and ρ (–)	Predicted Strength Limit State Sequence
Top Chord	End Panel	0.90	0.54		0.59		0.45	
	Interior Panel		0.87	Secondary	0.88	Secondary	0.87	Secondary
Bottom Chord		1.00	0.99	Primary	0.95		1.00	Primary
End Web	P1		1.00		1.00	Primary	0.92	
Interior Primary Web	P2	0.80	0.63		0.70		0.72	
	P3	0.95	0.63		0.81		0.43	
	P4	0.80	0.64		0.68		0.57	
	P5	0.95	0.40		0.54		0.36	
	P6	0.80	0.53		0.77		0.75	
	P7	0.95	0.24		0.66		0.28	
	P8	0.80	0.44				0.59	
	P12	0.80					0.77	

was braced at the third points to replicate transverse cross-bridging applied to joist systems. The bottom-chord center panels and both end webs were painted with lime wash to identify yielding during testing. During testing, load was applied at an approximate rate of 1,000 lb/min. Fifty-kip capacity load cells were placed at each support (Figure 1) to capture the total load applied to the system. A linear variable differential transducer (LVDT) recorded the deflection of the bottom chord at mid-span (Figure 1). Load and displacement were recorded at a sampling rate of 10 Hz using a 16-bit data acquisition system.

Sample details are shown in Figure 2. The K-series samples (Figure 2a) featured continuously crimped (CC), single-angle web members, which are characterized by bending the outermost region of each leg to fit and align the angle centroid in the same plane as the centroid of the chords. The larger LH-series samples (Figure 2b) featured a combination of continuously crimped, single-angle and double-angle web members. The rod-web K-series samples (Figure 2c) consisted of a continuous round bar bent at the panel points to form the web members. Also, the P2 and P4 compression webs were fabricated as rods reinforced with single angles, and the corresponding design strength for these reinforced members was used in determining the relative strength factors of Table 3.

All experimental joist samples were designed for a ductile limit state using an assumed yield strength (F_y) of 50 ksi and by the limiting relative strength factors described earlier (i.e., compression-web $\rho_{max} = 0.80$, top-chord $\rho_{max} = 0.90$, interior-tension web $\rho_{max} = 0.95$, bottom-chord and end-web $\rho_{max} = 1.00$). Table 3 presents maximum relative strength factors (ρ_{max}), member stress ratios (SR) and member relative strength factors (ρ) for the three joist series fabricated and tested in this study. For K-series samples, tensile yielding of both the bottom chord and end web is predicted as the relative strength factor for each at 1.00. This will be followed by top-chord buckling (ρ = 0.87). The controlling compression-web relative strength factor is 0.64 for member P4, so that web buckling is unlikely. For LH-series, ductile yielding of the end web is predicted (ρ = 1.00). Bottom-chord yielding (ρ = 0.95) could occur before achieving a secondary limit state of top-chord buckling (ρ = 0.88). Compression-web buckling is controlled by member P6 with ρ = 0.77 and is unlikely to occur before top-chord buckling. For the rod-web K-series joists, bottom-chord yielding is predicted (ρ = 1.00), followed by top-chord buckling (ρ = 0.87). Compression-web strength is controlled by P12 with ρ = 0.77. The over-strength on the compression web predicts top-chord buckling as the secondary limit state for the rod web joists.

The SJI-factored LRFD design loads determined by Equations 2 through 6 for the ductile joists detailed in Figure 2 are 418 lb/ft for the 20-in.-deep ductile K-series, 1303 lb/ft for the 28-in.-deep ductile LH-series and 420 lb/ft for the 16-in.-deep ductile rod-web K-series. In comparison to standard joists of equal span that are designed for the same factored loads but with no preference for controlling the strength limit state, the ductile joists weigh about 8% more. A significant amount of this weight increase is related to the top-chord size, where over-strength related to the design

limit of $\rho \leq 0.90$ requires a larger section. It should be understood, however, that the 8% weight increase noted is specific to the joists tested in this study and that, in general, the weight increase associated with the ductile design methodology will vary with many factors, such as span length, joist type, material availability and manufacturer.

The actual yield strength of the bottom-chord material was experimentally measured using the procedures of ASTM E8-04b, *Standard Test Methods for Tension Testing of Metallic Materials* (ASTM, 2004). For each of the 18 joists tested, a coupon was removed from the bottom-chord end panel. This location (bottom-chord end panel) was selected because of the low stress in this length. From test results, the average yield strength for the J1, J2 and J3 samples was found to be 60.3, 60.6 and 61.5 ksi, respectively. Thus, the measured yield strength is about 20% higher than was used for design. Significantly, unusually high yield strength may defeat the onset of tensile yield and ductile behavior. However, in the event of yield strength high enough to preclude the desired tensile yielding limit state, the use of relative over-strength factor, ρ, on the compression members would ensure strength in excess of a joist designed in accordance with SJI (2010).

TEST RESULTS

In preparation for testing to collapse, all joists were first preloaded to a nominal displacement of 1 in., or about 40% of the LRFD factored design load. This was done to ensure that all data acquisition was functioning properly and to seat the test sample in the loading frame, thereby removing any gap deformation among the loading apparatus, joist sample and supports. Upon release of the preload, the data acquisition system was zeroed and testing to failure commenced. Results for the K-series, LH-series and rod-web K-series are shown in Figure 3, where it is noted that the horizontal axis is center-span deflection and the vertical axis is the equivalent uniformly distributed load (w) determined as the total hydraulic force (P_{total}) divided by 32 ft ($w = P_{total}/32$ ft) Also, the load axis in Figure 3 includes the dead weight of the testing apparatus and self-weight of the joist, which are simply added to the force applied by the hydraulic cylinders. The total dead load was determined by weighing all components of the system in the absence of hydraulic force.

As can be seen from Figure 3, initial response for all joists is elastic with a linear load-deflection response, indicating all member stresses below yield. For each of the three joist

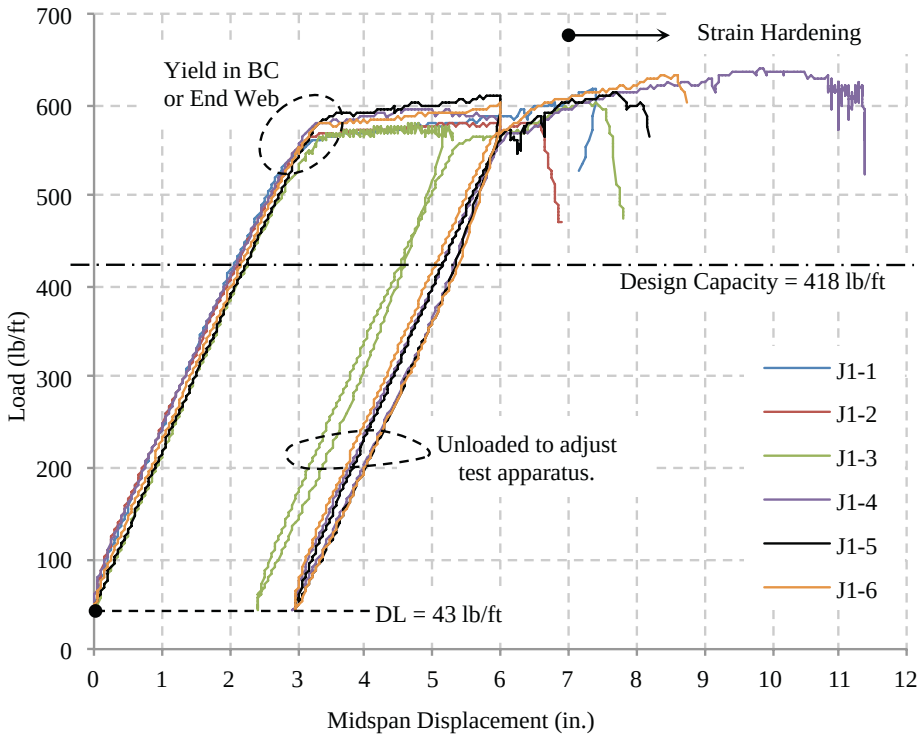

(a) K-Series

Fig. 3. Load-displacement results: (a) K-series (continued next page).

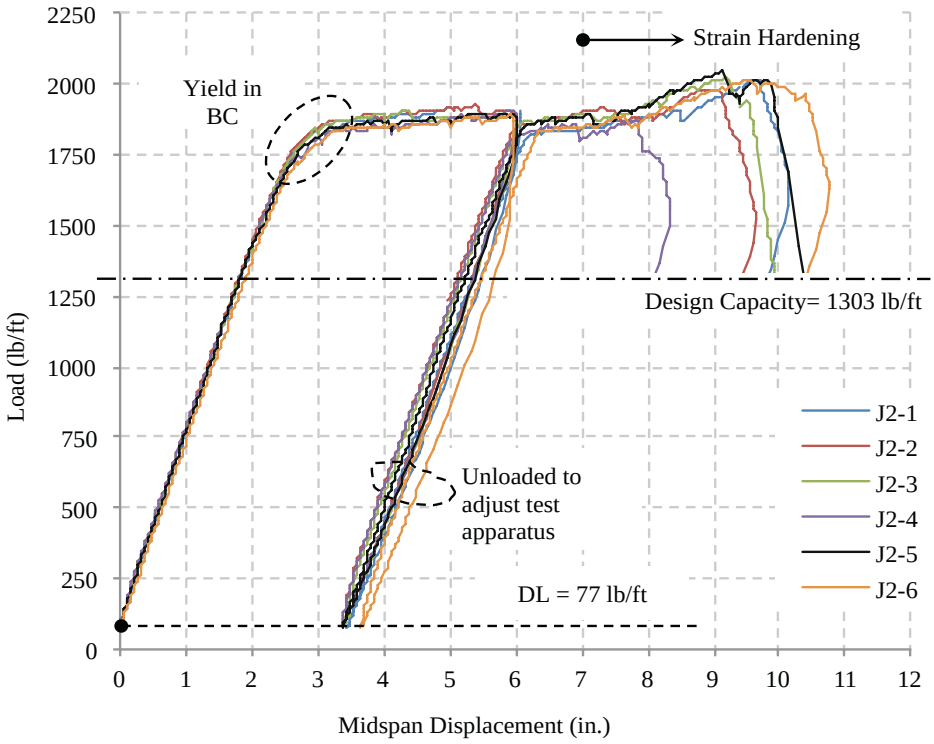

(b)

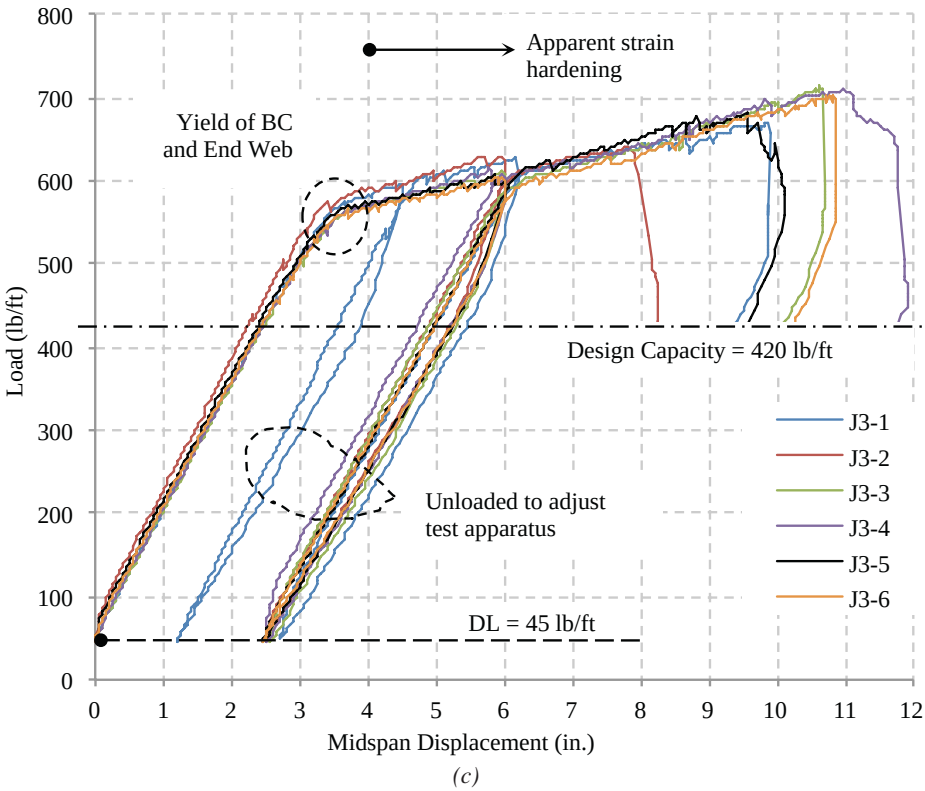

(c)

Fig. 3 continued. Load-displacement results: (b) LH-series; (c) rod-web K-series.

series, a high degree of repeatability is evident among the six identical samples. As the extreme fiber stress of the critical tension member reaches yield, the behavior transitions from elastic to inelastic, as is evident in the accelerated deflection rate and curvature of the load-deflection response. For all joist specimens, first yield occurred at the bottom-chord mid-span location and was visually identified by flaking of lime wash at that location. Typical bottom-chord yielding and lime-wash flaking can be seen in Figure 4a. Eventually, the critical tension member fully yields, and a plastic load plateau is achieved on the load-deflection response. For K-series and rod-web K-series, yielding of the end web was also detected, as shown in Figure 4b. No end-web yield was detected in the LH-series samples.

Following the fully plastic condition, all joists were loaded to approximately 6 in. of deflection and subsequently unloaded. The residual deflection is noted in Figure 3 and ranges from about 2.5 to 3.5 in. Unloading at 6 in. of deformation was necessary to reset the LVDT to a lower position and capture the full deformation of the joist, which would otherwise exceed the LVDT stroke capacity. The joists were then reloaded, resuming the load plateau and continued plastic deformation. Stiffness of the reloading branch was nearly identical to stiffness of the initial elastic response. All joists were loaded to collapse, which occurred by compression-member buckling of either the top chord or a web member. Table 4 summarizes test results in terms of load and displacement at yield (Y), plastic (P) and ultimate (U), as well as the secondary strength limit state and various ratios. In Table 4, yield (Y) is taken at initial departure from linear-elastic behavior; plastic (P) is defined as the load plateau, which is taken at 4 in. of joist displacement; and ultimate (U) is the secondary strength limit state of compression-member buckling. Figure 5 presents results graphically in terms of ultimate-displacement-to-yield-displacement or ductility ratio (Figure 5a) and average load ratios at yield, plastic and ultimate relative to the ductile design capacity (Figure 5b). Individual series results are discussed in the following sections.

K-Series Discussion (Samples J1-1 through J1-6)

The predicted failure mode for these joists is given in Table 3 and expected to be simultaneous yielding of the end web and bottom chord ($\rho = 0.99$ and 1.00), followed by top-chord buckling ($\rho = 0.87$). The failure behavior observed during testing is consistent with this prediction. As mentioned, flaking of lime wash, indicating yielding, was observed on the bottom-chord and end-web members. Bottom-chord yielding was observed to initiate adjacent to the panel points of the bottom-chord mid-span segment (B4). As inelastic displacement increased, the bottom chord yielded region spread down the length of panel B4 (Figure 4d). At ultimate load capacity, the complete cross-section of the bottom-chord B4 panel for the entire member length showed evidence of yielding; however, no yield was detected in the neighboring bottom-chord panels (B3 and B5). End-web yielding generally occurred after significant bottom-chord yielding and was evident over approximately the middle half of both end-web members.

After significant plastic deformation, each sample experienced top chord buckling. In general, top-chord buckling occurred between brace points and about the *y*-axis, or out of the plane of the joist, characterized by an unrecoverable drop in load-carrying capacity. A typical top-chord buckling condition is shown in Figure 4c. For sample J1-2, the load distribution unit was rotated out-of-plane, inducing an eccentric load on the top chord and promoting premature buckling. Thus, strength and deformation at ultimate of this sample are not considered in Table 4. For samples J1-1, J1-4 and J1-6, there appears to be a region of strain hardening after approximately 7 in. of deflection (Figure 3a). This is evident in the slight increase in load after the plastic load plateau.

Excluding sample J1-2, deformation at ultimate ranged from 7.37 in. (sample J1-1) to 10.8 in. (sample J1-4). In terms of span length, this represents $L/54$ to $L/37$, a tremendous amount of deformation. Ductility results in Table 4 and Figure 5a show a range from 2.47 (sample J1-5) to 3.55 (sample J1-4) with a series average of 2.83, demonstrating a significant amount of energy dissipation in the form of inelastic deformation. Average strength ratios in Figure 5b show progressively increasing capacity at yield, plastic and ultimate relative to design, and strength ratio standard deviations are all very low (Table 4). Specifically, the yield-strength-to-design-strength ratio (Y/D in Table 4 and Figure 5b) ranges from 1.23 to 1.34, with a series average of 1.29, and ultimate-strength-to-design-strength ratio (U/D in Table 4 and Figure 5b) ranges from 1.45 to 1.52, with a series average of 1.49. The strength ratios and associated standard deviations indicate predictable behavior with low variability, conservative design relative to the primary strength limit state of tensile yield and substantial reserve strength relative to the secondary strength limit state of compression buckling.

LH-Series Discussion (Samples J2-1 through J2-6)

The predicted strength limit state for these joists is given in Table 3 and expected to be end-web yielding ($\rho = 1.00$) followed by secondary buckling of the top chord ($\rho = 0.88$). The bottom chord has a ρ of 0.95 and may yield prior to a compression-member buckling. The observed behavior was not consistent with this prediction. Rather, in all six cases, yielding occurred on the bottom chord only, initiating on either side of the mid-span panel point, as shown in Figure 4e. Bottom chord yielding was observed simultaneously in both members adjacent to the mid-span panel point (B3 and B4). As deformation increased, bottom-chord yielding

Table 4. Summary of Test Results

		Yield (Y)		Plastic (P)		Ultimate (U)			Ratio P/Y		Ratio U/Y		Design Load Ratio[b]		
Series	Sample	Load (lb/ft)	Disp. (in.)	Load (lb/ft)	Disp. (in.)	Secondary Strength Limit State[a]	Load (lb/ft)	Disp. (in.)	Disp. (–)	Load (–)	Disp. (–)	Load (–)	Y/D (–)	P/D (–)	U/D (–)
K-Series	J1-1	515	2.67	568	4.00	TCB	620	7.37	1.50	1.10	2.76	1.20	1.23	1.36	1.49
	J1-2	538	2.90	574	4.00	LAC			1.38	1.07			1.29	1.38	
	J1-3	512	2.86	567	4.00	TCB	604	7.40	1.40	1.11	2.59	1.18	1.23	1.36	1.45
	J1-4	559	3.04	589	4.00		634	10.8	1.32	1.05	3.55	1.13	1.34	1.41	1.52
	J1-5	557	3.12	592	4.00		614	7.72	1.28	1.06	2.47	1.10	1.34	1.42	1.47
	J1-6	558	3.08	582	4.00		634	8.57	1.30	1.04	2.78	1.14	1.34	1.39	1.52
	Average	540	3.00	579	4.00		621	8.37	1.36	1.07	2.83	1.15	1.29	1.39	1.49
	Std. Dev.	22	0.17	11	0.00		13	1.44	0.08	0.03	0.42	0.04	0.05	0.03	0.03
LH-Series	J2-1	1670	2.43	1878	4.00	TCB	2019	9.62	1.65	1.12	3.96	1.21	1.28	1.44	1.55
	J2-2	1671	2.41	1882	4.00	TCB & S4B	1982	9.03	1.66	1.13	3.75	1.19	1.28	1.44	1.52
	J2-3	1721	2.54	1886	4.00	TCB	2026	9.19	1.57	1.10	3.62	1.18	1.32	1.45	1.56
	J2-4	1648	2.40	1852	4.00		1864	7.82	1.67	1.12	3.26	1.13	1.27	1.42	1.43
	J2-5	1640	2.41	1868	4.00	TCB & S4B	2013	9.83	1.66	1.14	4.08	1.23	1.26	1.43	1.55
	J2-6	1617	2.43	1855	4.00	TCB	2004	9.86	1.65	1.15	4.06	1.24	1.24	1.42	1.54
	Average	1661	2.44	1870.2	4.00		1985	9.23	1.64	1.13	3.79	1.20	1.28	1.44	1.52
	Std. Dev.	36	0.05	14.43	0.00		61	0.77	0.03	0.02	0.32	0.04	0.03	0.01	0.05
Rod-web K-Series	J3-1	523	3.12	582	4.00	PWB	667	9.89	1.28	1.11	3.17	1.28	1.25	1.39	1.59
	J3-2	541	3.09	589	4.00	TCB	638	7.82	1.29	1.09	2.53	1.18	1.29	1.40	1.52
	J3-3	512	3.10	567	4.00	PWB	709	10.65	1.29	1.11	3.44	1.39	1.22	1.35	1.69
	J3-4	518	3.14	568	4.00	TCB	703	11.08	1.27	1.10	3.53	1.36	1.23	1.35	1.68
	J3-5	531	3.18	572	4.00	PWB	679	9.54	1.26	1.08	3.00	1.28	1.26	1.36	1.62
	J3-6	539	3.35	566	4.00	PWB	698	10.86	1.19	1.05	3.24	1.29	1.28	1.35	1.66
	Average	527	3.16	574	4.00		682	9.97	1.27	1.09	3.15	1.30	1.26	1.37	1.63
	Std. Dev.	12	0.10	9	0.00		27	1.21	0.04	0.02	0.36	0.07	0.03	0.02	0.06

[a] LAC = load apparatus complication, TCB = top-chord buckling, S4B = S4 web buckling, PWB = primary web buckling

[b] LRFD Factored Design Load (D) K-series = 418 lb/ft, LH-series = 1303 lb/ft, Rod-web K-series = 420 lb/ft

spread down the length of the B3 and B4 panels. However, no end-web yielding occurred in any of the samples. The LH-series end webs are double-angle members with battens welded to the third points. The end webs did not yield as predicted, possibly due to a higher yield strength than the bottom chord. At approximately 7.0 in. of deformation, a region of strain hardening occurred (Figure 3b) where the load capacity gradually increased until ultimate collapse under the secondary strength limit state of compression-member buckling.

The secondary strength limit state for samples J2-2 and J2-5 was a combination of buckling of the S4 web member followed by buckling of the top chord at center span. The S4 web buckling was not a sudden condition, rather a deformed bent shape of the member was evident as the joist approached failure by top-chord buckling, as is shown in Figure 6a. The deformed shape of the S4 web only occurred at very high deflection, in excess of approximately 7 in. At ultimate collapse, top-chord buckling was out of the plane of the joist for sample J2-2. For sample J2-5, top-chord buckling occurred in the plane of the joist between the two panel points located 28 in. on either side of center span. Simultaneous buckling of the S4 member was also observed, which resulted in the loss of in-plane bracing by the S4 web at center span on the top chord. This behavior is shown in Figure 6b. For the remaining four LH-series samples, some evidence of S4 buckling or bending was observed; however, ultimate collapse occurred by top-chord buckling out of the plane of the joist at an interior panel.

The S4 member is a secondary vertical web member and is not predicted by elastic analysis to be highly stressed by direct application of externally applied loads. The elastic analysis is based on relatively small deformations where the S4 member force is largely based on tributary loading, as is shown in Figure 7a. Secondary web members are generally not important force-resisting members, but rather primarily provide in-plane bracing for the top chord. However, considering its location at the highly stressed top-chord

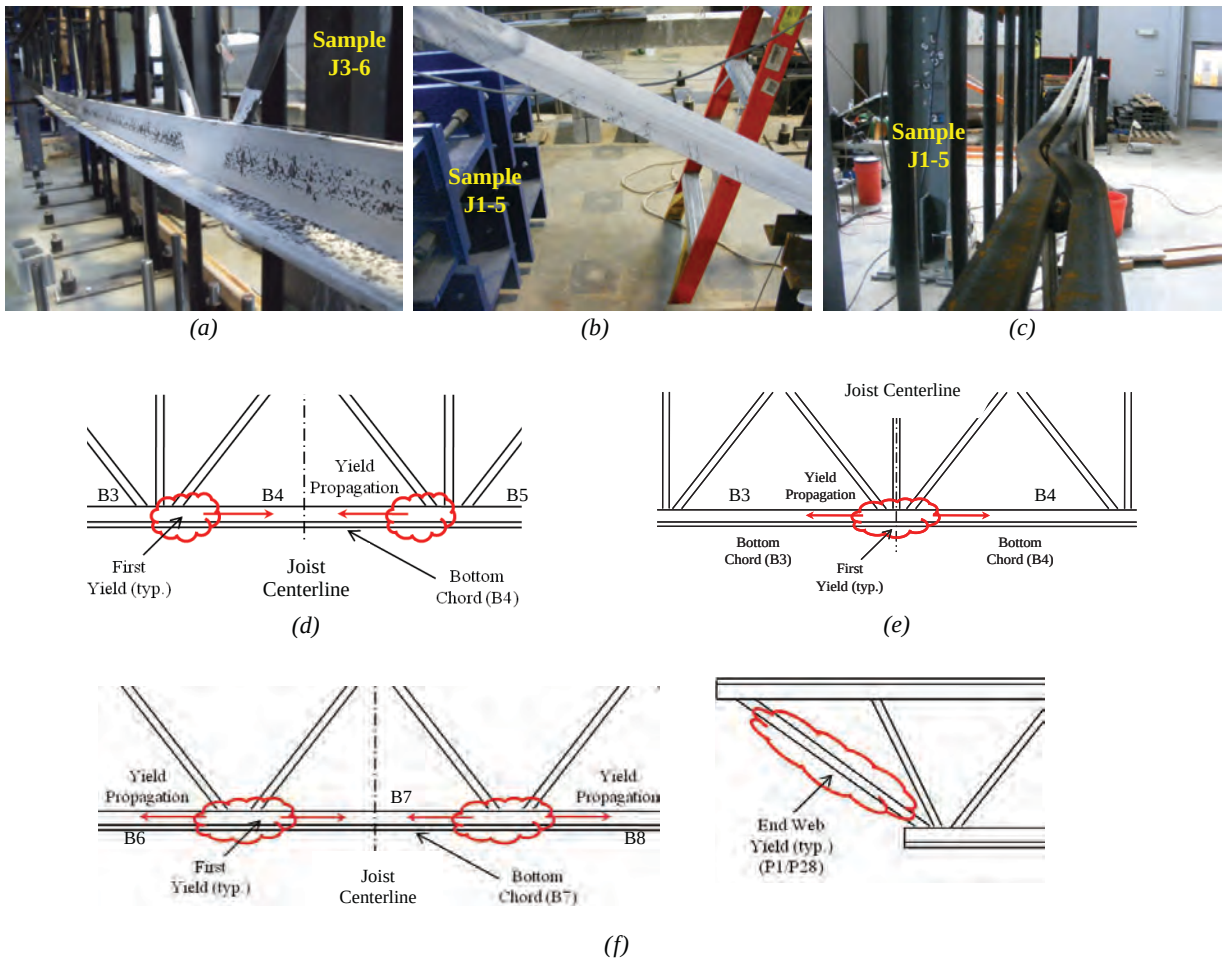

Fig. 4. Member yielding and buckling: (a) bottom-chord yielding; (b) end-web yielding; (c) top-chord buckling; (d) bottom-chord yielding in K-series samples; (e) bottom-chord yielding in LH-series samples; (f) bottom-chord and end-web yielding in rod-web K-series samples.

mid-panels, test results show that the S4 member appears to become highly stressed under extreme inelastic joist displacement. This condition likely results from the very large vertical deformation and corresponding development of a vertical force component in the top-chord axial force that, by joint equilibrium, acts on the vertical web, as shown in Figure 7b. This results in stresses well beyond those calculated for elastic behavior and small deformations. Currently, the SJI requires only that vertical web members be designed for gravity load plus 0.5% of the top-chord axial force (SJI, 2010). This requirement should be reexamined with consideration of ensuring that vertical-web members possess the necessary strength required to resist axial forces associated with large deformation behavior. It should be noted that this behavior was only evident after the test joists had successfully demonstrated the intended goal of extreme inelastic ductile deformation while retaining full load-bearing capacity and that the vertical web buckling was not sudden in nature.

Ductility results of Table 4 and Figure 5a show that the LH-series achieved the highest performance of the three series tested. Ductility ranged between 3.26 (sample J2-4) and 4.08 (sample J2-5), with a series average of 3.79. The high ductility ratios appear to result in a strain-hardening region that begins at approximately 7 in. of deformation, approximately three times the yield displacement. At these high deflections, strain hardening in the yielding tension member is achieved, resulting in the tangent stiffness apparent in the test results. This strain hardening behavior is further supported by the load-strain results for sample J2-6 shown in Figure 8, where strain data were collected at the middle length of both end webs, as well as the bottom chord

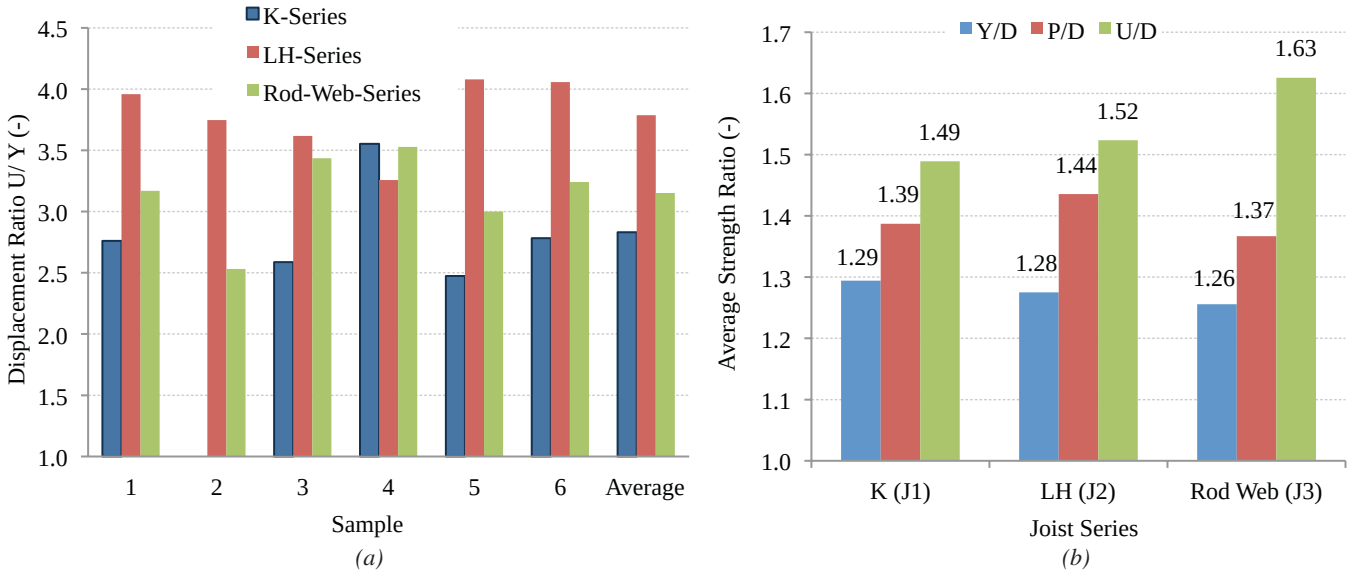

Fig. 5. Ratio results (a) ductility ratio; (b) average strength ratios.

Fig. 6. Secondary limit state failure for J2 and J3 series: (a) sample J2-2; (b) sample J2-5; (c) sample J3-1; (d) sample J3-5.

at center span. Figure 8 shows that the end webs remained elastic (SG1, SG2, SG5, SG6), but there is severe yielding in the bottom chord (SG3, SG4). The strain at yield is measured to be about 2,100 microstrain, after which there is a sharp transition to a perfectly plastic condition. At about 16,000 microstrain, strain hardening initiates and continues to about 19,500 microstrain, at which point secondary compression-member buckling occurs. After testing, the bottom chords were all visually inspected and measured with a digital caliper, and there was no visible or measurable evidence of a reduced cross-section or necking.

Average strength ratios in Figure 5b show progressively increasing capacity at yield, plastic and ultimate relative to design and also indicate strength ratio standard deviations are all very low (Table 4). The yield-strength-to-design-strength ratio (Y/D in Table 4 and Figure 5b) ranges from 1.24 to 1.32, with a series average of 1.28, and ultimate-strength-to-design-strength ratio (U/D in Table 4 and Figure 5b) ranges from 1.43 to 1.56, with a series average of 1.52. As with the K-series joists, strength ratios and associated standard deviations indicate predictable behavior with low variability, conservative design relative to the primary

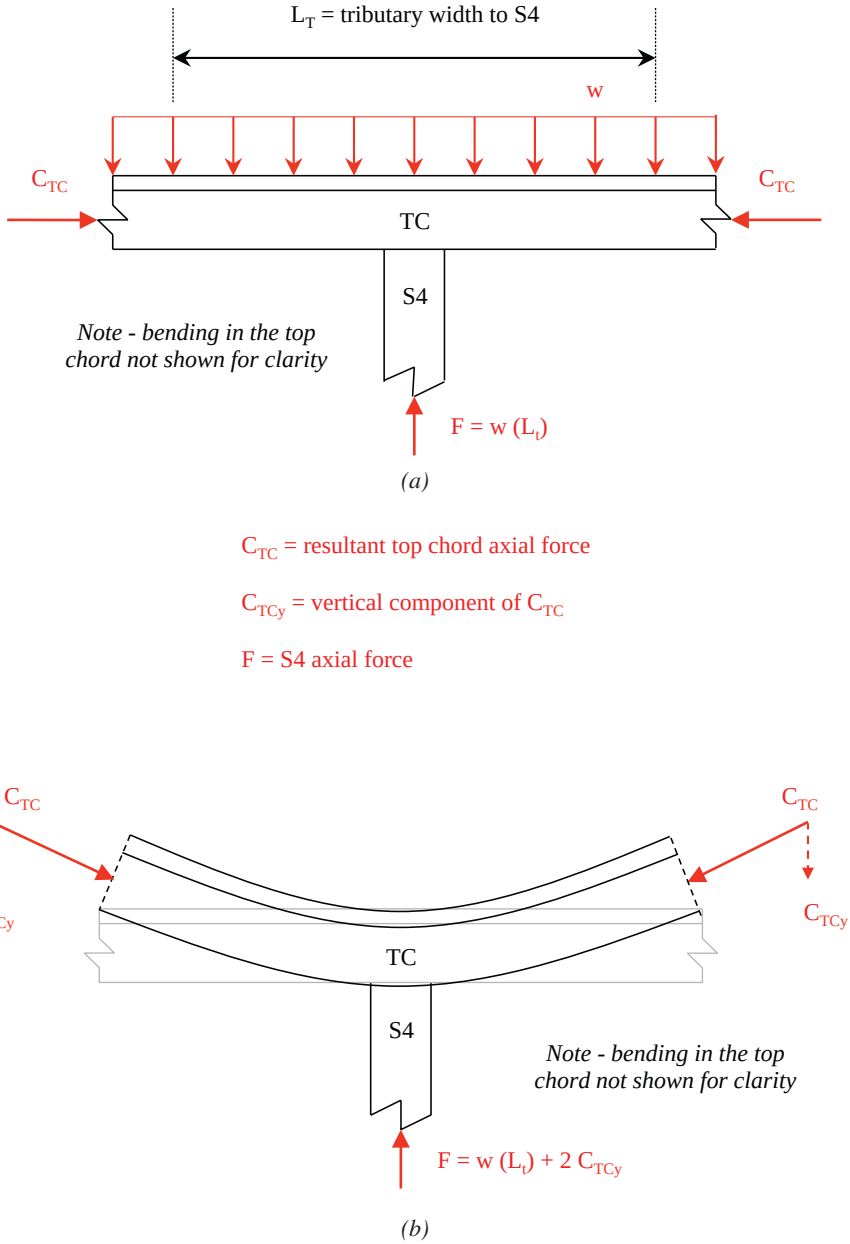

Fig. 7. S4 member axial force: (a) small deformation; (b) large deformation.

strength limit state of tensile yield and substantial reserve strength relative to the secondary limit state.

Rod-Web K-Series Discussion (Samples J3-1 through J3-6)

The predicted strength limit state sequence for these joists as provided in Table 3 is bottom-chord yielding ($\rho = 1.00$) followed by top-chord buckling ($\rho = 0.87$). Yielding of the end web before top-chord buckling is possible with $\rho = 0.92$. The load-deflection results for the rod-web K-series joists are shown in Figure 3c, where extreme ductile behavior is noted. For all samples, response is initially elastic followed by bottom-chord yielding. The observed yielding result is consistent with predicted behavior. In all cases, first yielding occurred in the bottom-chord mid-span panel (B7). This mechanism was observed to start adjacent to the panel points on each side of the B7 panel, as is shown in Figure 4f. As inelastic displacement increased, yielding spread down the length of the B7 panel as well as into adjacent bottom-chord panels (B6 and B8). At very high displacements, lime-wash flaking was also observed in the B5 and B9 panels. After the onset of bottom-chord yielding, end-web yielding was also observed. In some instances, the end-web yielding was observed over the entire cross-section and length of the end bars (Figures 4f and 6c).

After full, bottom-chord yielding, the behavior appears to directly enter a strain-hardening region (Figure 3c). This is evident in the absence of a horizontal load plateau following full yielding of the bottom chord. Rather, there is an immediate resumption of load increase, albeit at a much reduced rate. The load versus displacement plot of Figure 3c shows an inclined yield plateau, indicating an increase in strength as deflections increase. This behavior was attributed to strain hardening after about 7 in. of deflection in the K-series and LH-series joists (Figures 3a and 3b); however, for the rod-web K-series, its onset is immediate and continuous throughout the loading from first yield to ultimate collapse. This appears to be the result of more numerous rod-web members relative to the geometric layout of deeper joists. With the spacing between panel points minimized, the stress redistribution can occur more continuously as the bottom-chord member is yielding.

At secondary limit state, only two of the six joists (J3-2 and J3-4) experienced the top-chord buckling anticipated by the theoretical failure sequence. The top-chord buckling locations were confined to the central panels (T7 through T10). Three specimens (J3-1, J3-3, J3-6) collapsed in buckling of the first interior compression web member (P2/P27), which is a ⅝-in.-round bar reinforced with a 1 in. × 1 in. × 0.109 in. angle. In each of these cases, the buckled web member was adjacent to an end web member that demonstrated substantial yielding prior to buckling. These types of failure are shown in Figure 6c. The J3-5 specimen had a relatively unique secondary limit state of buckling in the P8/P21 and P6/P23 compression web members, as shown in Figure 6d. While not necessarily expected, their ultimate buckling is understandable in that they are the first unreinforced compression bars from the end of the joist and have design stress ratios of 0.59 and 0.75, respectively.

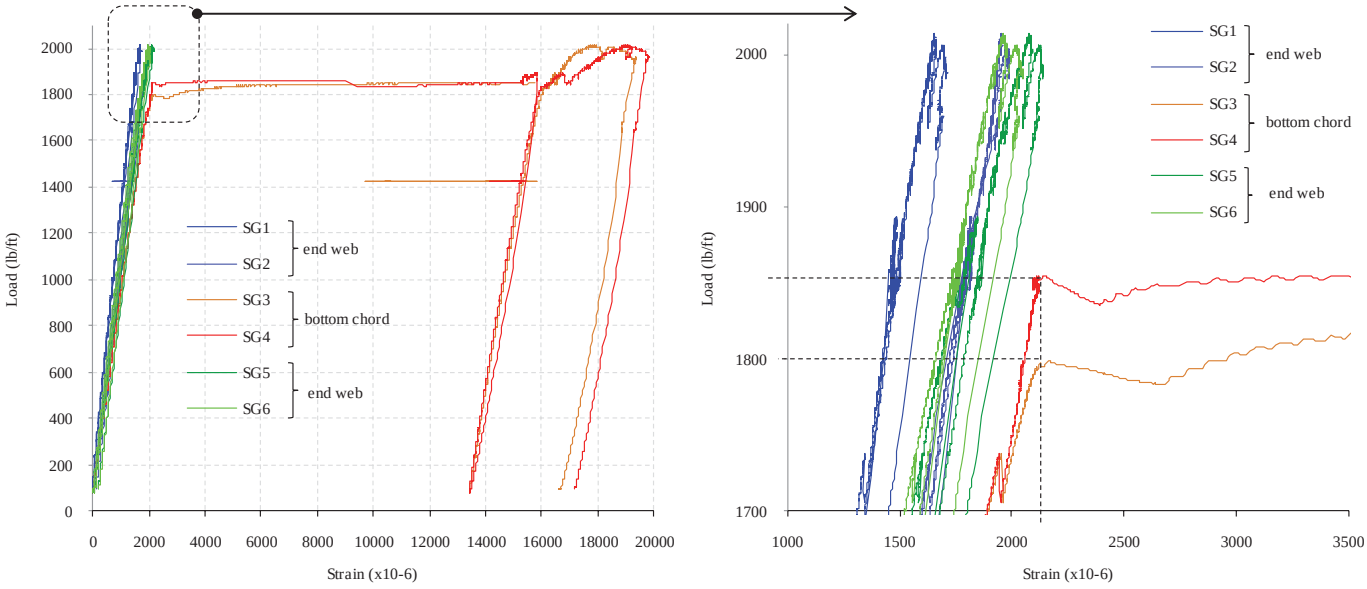

Fig. 8. Tension-member strain results for sample J2-6.

Ductility ratios from Figure 5a range from 2.53 for sample J3-2 to 3.53 for sample J3-4, with a series average of 3.15. As with J1 and J2 samples, average strength ratios in Figure 5b show progressively increasing capacity at yield, plastic and ultimate relative to design, and strength ratio standard deviations are all very low (Table 4). The yield-strength-to-design-strength ratio (Y/D in Table 4 and Figure 5b) ranges from 1.22 to 1.29, with a series average of 1.26, and ultimate-strength-to-design-strength ratio (U/D in Table 4 and Figure 5b) ranges from 1.52 to 1.69, with a series average of 1.63. The strength ratio U/D is the highest of the three joist series tested, and represents additional strength developed from the post-yield inclined load plateau (Figure 3c). As with the K-series and LH-series joists, strength ratios and associated standard deviations indicate predictable behavior with low variability, conservative design relative to the primary strength limit state of tensile yield and substantial reserve strength relative to the secondary limit state.

DISCUSSION OF TEST RESULTS AND RELABILITY INVESTGATION

The ductile design methodology related to controlling member strength by implementation of the relative strength factor ρ in member selection (all as summarized in Table 1) is fully supported by 18 experimental data points.

For each joist tested, the intended ductile behavior was achieved and characterized by tension yield, followed by significant plastic deformation and ultimate failure by compression buckling. Thus, the ρ factors selected for design provided sufficient compression-member over-strength, allowing tensile yield as the initial strength limit state and, importantly, yield and ultimate collapse at strengths well in excess of the predicted design capacity. As well, the experimental test results are uniquely significant when measured relative to the design limit state (D) at each the yield (Y) or primary strength limit state, plastic limit state (P) and ultimate (U) or secondary strength limit state conditions. That is, experimental behavior is characterized by three unique limit states that occurred sequentially with increasing strength capacity in all 18 samples (Figure 5b). Ultimately, these three limit states (Y, P and U) are a predictable sequence, where the plastic limit state represents an important transition from the primary to the secondary strength limit states. Strength ratios and corresponding statistical data are important in this discussion as well. As is seen in Table 4 and Figure 5b, the strength ratios at each of the yield, plastic and ultimate conditions relative to LRFD ductile design capacity are progressively increasing, with each ratio having a significant factor of safety and low standard deviation. This ensures a conservative design with the primary strength limit state corresponding to the yield limit condition, significant residual strength at the secondary limit state and low variability for all three strength ratios.

Although an in-depth reliability study is beyond the scope of this paper, the reduced variance in the strength of members in tension relative to the strength of slender members in compression results in improved reliability and is worth exploring as an extension of the test results presented. If materials purchased for the bottom chord and end webs are limited to a specific steel alloy supplied by a specific mill, further reductions in variance can be found, resulting in more reliable strength and limit state control. Accordingly, an exploratory reliability investigation has been performed based on the tested joist plastic strengths (P), together with merchant bar steel mill test data, and employing the criteria and assumptions used to develop the 2005 AISC LRFD design approach. Merchant bar steel mill test data have been furnished by Steel Dynamics Roanoke Bar Division, for ASTM A529-50 steel, covering a time frame from May 2008 to October 2012 (Steel Dynamics, 2012). In all, the data included 11,546 test samples representing 4,337 batches of steel. The yield stress population distribution and statistical data for these 11,546 samples are provided in Figure 9. For joist test strength ratios, the 18 tested joist plastic strengths have been divided by the joist experimental design strength, which is defined as the nominal strength times the ratio of member tested F_y to specified minimum F_y (50 ksi). A summary of these loads and ratios is provided in Table 5. Lacking data for broad comparisons of actual section properties to nominal section properties, the industry standard data published in Table F1 of AISI 2007 (AISI, 2007) have been used for these ratios.

The LRFD design approach used by both the 2005 AISC *Specification* and the 2007 AISI design specification follows the equations and procedures presented in a series of eight articles in the September 1978 issue of the *Journal of the Structural Division*. However, the two differ in the ratio of live-to-dead loads used for calibration of LRFD to the historical ASD design method. For LRFD calibration, the 2005 AISC *Specification* uses a live-to-dead load ratio of 3, whereas AISI uses a live-to-dead load ratio of 5. From AISI Chapter F, *Tests for Special Cases,* and Commentary on Chapter A, *General Provisions*, the relative reliability index is calculated as:

$$\beta = \frac{\ln\left[\frac{C_\phi}{\phi}(M_m F_m P_m\right]}{\sqrt{V_M^2 + V_F^2 + C_P V_P^2 + V_Q^2}} \tag{8}$$

where

β = relative reliability index
ρ = resistance factor = 0.90
C_ϕ = calibration coefficient, which may be shown [using procedures demonstrated in AISI (2007) Commentary on Chapter A, *General Provisions*] to equal 1.481 for LRFD with live-to-dead load ratio of 3

M_m = mean value of material factor, M
= 1.135 from Steel Dynamics Roanoke Bar Division data for ASTM A529-50 merchant bar (see Figure 9)
F_m = mean value of fabrication factor, F
= 1.0 from AISI (2007) Table F1
P_m = mean value of professional factor, P, for tested component
= 1.033 from test-average-plastic-to-experimental-design ratio (see Table 5)
V_M = coefficient of variation of material factor
= 0.0602 from Steel Dynamics Roanoke Bar Division data for ASTM A529-50 merchant bar (Figure 9)
V_F = coefficient of variation of fabrication factor
= 0.05 from AISI 2007 Table F1
C_P = correction factor
= 1.196 for 18 test samples
V_P = coefficient of variation of joist test results
= 0.029 from test results data (see Table 5)
V_Q = coefficient of variation of load effect, which may be shown (using procedures demonstrated in AISI (2007) Commentary on Chapter A, *General Provisions*) to equal 0.187 for LRFD with live-to-dead load ratio of 3

Substitution of these values into Equation 8 yields an approximate plastic strength $\beta = 3.2$. This is an improved reliability as compared to the approximate $\beta = 2.6$ for members, reported in the 2005 AISC *Specification* and reflective of expectations of a joist designed in accordance with the SJI standard (2010). It should be noted that the calculated approximate plastic strength $\beta = 3.2$ is based on the joist tested plastic limit state (Tables 4 and 5), above which the joists demonstrated consistent reserve capacity before attaining ultimate maximum load capacity.

In summary, the ductile design methodology employed in this experimental program produced the predicted behavior related to achieving ductile failure, resulting in a slow collapse mechanism characterized by large inelastic deformation and improved reliability. The loss in economy is acknowledged as a consequence of adjusting member strengths.

CONCLUSIONS AND FINDINGS

The research presented in this study experimentally explores a design methodology for open-web steel joists, where the primary strength limit state is ductile tensile yielding of the bottom chord or end web, which, after significant inelastic

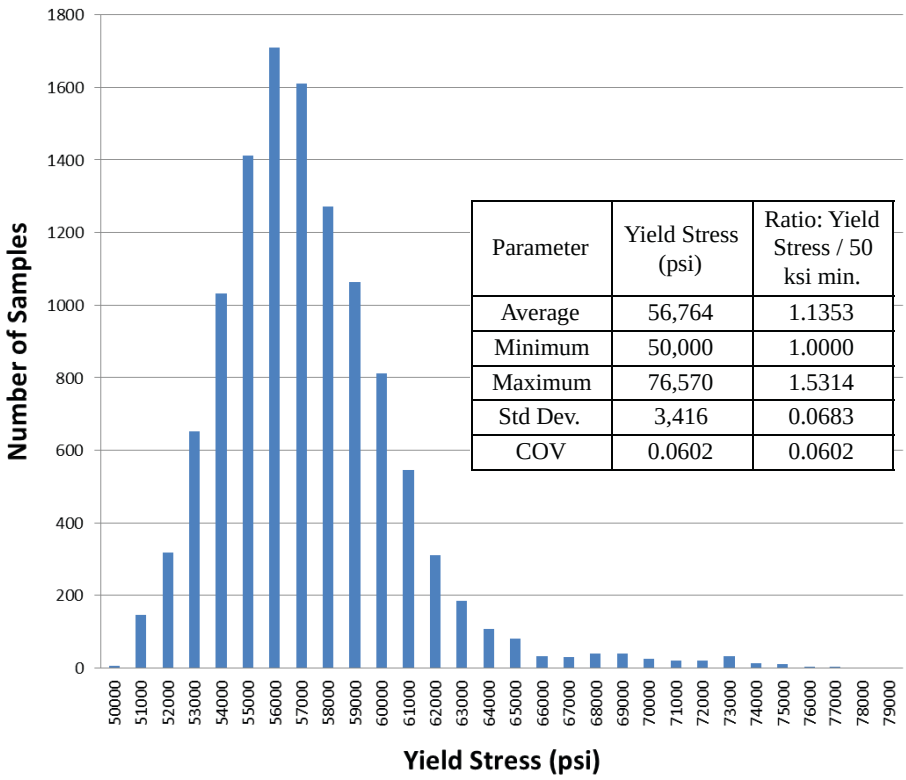

Parameter	Yield Stress (psi)	Ratio: Yield Stress / 50 ksi min.
Average	56,764	1.1353
Minimum	50,000	1.0000
Maximum	76,570	1.5314
Std Dev.	3,416	0.0683
COV	0.0602	0.0602

Fig. 9. Yield stress population distribution and statistical data.

Table 5. Statistical Data for Joist Tests						
Series	**Sample**	**SJI LRFD Design Load (lb/ft)**	**F_y Experimental (ksi)**	**Experimental Design Load (lb/ft)**	**Plastic Strength (lb/ft)**	**Ratio Plastic/ Exp Design Load (–)**
K-Series	J1-1	418	60.3	560	568	1.01
	J1-2				574	1.02
	J1-3				567	1.01
	J1-4				589	1.05
	J1-5				592	1.06
	J1-6				582	1.04
LH-Series	J2-1	1303	60.6	1755	1878	1.07
	J2-2				1882	1.07
	J2-3				1886	1.07
	J2-4				1852	1.06
	J2-5				1868	1.06
	J2-6				1855	1.06
Rod-web K-Series	J3-1	420	61.5	574	582	1.01
	J3-2				589	1.03
	J3-3				567	0.99
	J3-4				568	0.99
	J3-5				572	1.00
	J3-6				566	0.99
All	Average					1.0330
	Std. Dev.					0.0302
	COV					0.0293
	Quantity					18

deformation, is followed by a secondary strength limit state of buckling of the top chord or compression web. Importantly, the study scope is restricted to gravity loading of simply supported K-series and LH-series joists, where the bottom chord and end webs are in tension and the top chord is in compression. For other load and support conditions, where the force sense in these members is different, the stated findings may not apply.

Ductile behavior was achieved by adjusting the relative design strengths of the individual tension and compression members so that tension yielding precedes compression-member buckling. Adjusting the individual member tension and compression strengths to the appropriate relative strength factors results in a predictable failure sequence characterized by ductile behavior and sufficient capacity to support SJI LRFD design loads. The proposed ductile design methodology was experimentally investigated in the design, manufacturing and testing of modified K-series, LH-series and rod-web K-series joists. For each joist series, six identical joists were tested, for a total of 18 tests. All joists were simply supported with a uniformly distributed loading pattern applied to the top chord. The lengths were either 32 or 33 ft, and the top chord was laterally braced at 2-ft intervals. The following conclusions are derived from the test results:

- All 18 joists behaved in a ductile fashion, as predicted, with tension yielding as the primary strength limit state followed by compression-member buckling as the secondary strength limit state. For K-series and rod-web K-series joists, both the bottom chord and end web experienced tension yielding. For the LH-series joists, only the bottom chord experienced yielding.

- For the joists tested in this research, implementation of the ductile design relative strength factors as the basis for member selection resulted in an 8% increase in weight as compared to a conventionally designed joist of equal span and capacity. In general, the weight increase

associated with implementation of the ductile design methodology will vary with many factors such as span length, joist type, material availability and manufacturer.

- The yield strength for all 18 samples exceeded the LRFD design strength by a significant amount. For K-series, LH-series and rod-web K-series joists, the six sample average yield loads were 1.29, 1.28 and 1.26 times the LRFD design load, respectively. Reference for this conclusion is made to Table 4 and Figure 5b. This indicates a conservative design relative to the primary yield strength limit state.

- The series average ultimate strength ratio, which is defined as the load at ultimate divided by the LRFD factored design load, is 1.49, 1.52 and 1.63 for K-series, LH-series and rod-web K-series joists, respectively. Reference for this conclusion is made to Table 4 and Figure 5b. This indicates substantial reserve strength relative to the secondary strength limit state.

- The average ductility ratio for six identical samples, which is defined as the deflection at ultimate divided by the deflection at yield, was 2.83, 3.79 and 3.15 for K-series, LH-series and rod-web K-series joists, respectively. For all 18 samples tested, this ratio ranged from 2.47 to 4.08. Reference for this conclusion is made to Figure 5a and Table 4.

- The relative reliability factor calculated using joist test results and statistical data from 11,546 merchant bar test samples was 3.2, an increase of 23% over the 2.6 used by current SJI LRFD methodology. Reference for this conclusion is made to Figure 9 and Table 5.

- For the K-series and LH-series joists, the yield limit state was followed by a horizontal load plateau. After significant deformation, the load plateau terminated, and these joists experienced a gradual increase in load capacity that is associated with strain hardening in the yielded tension member. Reference for this conclusion is made to Figures 3 and 8. Ultimate collapse occurred as a secondary limit state of buckling of the top chord or compression web.

- For rod-web K-series joists, the yield limit state was followed by an immediate resumption of increasing load-bearing capacity. The post-yield behavior was an inclined linear increase in loading until secondary compression failure. Ultimate collapse occurred as a secondary limit state of top-chord buckling or compression-web buckling. Reference for this conclusion is made to Figure 3c.

- In several of the LH-series joists, bending and buckling of the secondary S4 web at mid-span was observed. This occurred after very high inelastic deformation and is attributed to development of a vertical component to the resultant chord axial force that delivers a substantial compression force on the web. Reference for this conclusion is made to Figures 6a, 6b and 7.

In conclusion, the ductile design philosophy was successfully implemented using the relative strength factor (ρ) as the basis for member selection, ensuring sufficient compression member over-strength relative to tension-member yield strength.

ACKNOWLEDGMENTS

The authors are grateful to Commercial Metals Company Inc. for providing financial support and materials for this project and to Steel Dynamics Roanoke Bar Division for sharing statistical data from mill tests of ASTM A529-50 merchant bar. The authors also wish to thank the Villanova University Office of Research and Sponsored Projects for providing graduate tuition support and the Villanova University Center for Undergraduate Research and Fellowships for supporting an undergraduate researcher on this project.

SYMBOLS

A_g	= gross cross-sectional area
C_m	= moment factor
C_{TC}, C_{TCy}	= top-chord resultant force and vertical force component, respectively
C_P, C_ϕ	= correction factor and calibration coefficient, respectively
E	= elastic modulus
f_{au}	= factored axial stress
f_{bu}	= factored bending stress
f_u	= required member stress
F	= axial force in S4 web member
F_{cr}	= critical buckling stress
F_e	= Euler buckling stress
F_n	= nominal member stress at ultimate
F_y	= yield stress
F_m, M_m, P_m	= mean value of fabrication factor, material factor and professional factor, respectively
k	= effective length factor
L	= member length
L_t	= tributary length to top-chord panel point
M_u	= factored bending moment
P_u	= factored axial force
Q	= local buckling reduction factor
r	= radius of gyration
S	= section modulus
SR	= stress ratio
V_M, V_F, V_P, V_Q	= coefficients of variation for material, fabrication, joist test results and load effect, respectively
w	= applied distributed force pattern
β	= relative reliability index
ϕ	= strength reduction factor
ρ	= relative strength factor

REFERENCES

AISC (2005), *Specifications for Structural Steel Buildings,* 13th ed., American Institute of Steel Construction, Chicago, IL.

AISI (2007), *North American Specification for the Design of Cold-Formed Steel Structural Members*, American Iron and Steel Institute, Washington, DC.

ASTM (2004), "E8-04b Standard Test Methods of Tension Testing of Metallic Materials," ASTM E8-04b, American Society of Testing and Materials, West Conshohocken, PA.

Cianci, P.A., Yost, J.R., Gross, S.P. and Dinehart, D.W. (2009), "Design and Behavior of Ductile Open Web Steel Joists: Phase II," Research Report, Commercial Metal Corporation, Hope, AR.

Engelhardt, M.D., Kates, Z., Beck, H. and Stasney, B. (2000), "Experiments on the Effects of Power Actuated Fasteners on the Strength of Open Web Steel Joists," AISC, *Engineering Journal*, Fourth Quarter.

Iaboni, N.J., Yost, J.R., Gross, S.P. and Dinehart, D.W. (2007), "Design and Behavior of Ductile Open Web Steel Joists," Research Report, Commercial Metal Corporation, Hope, AR.

Rao, N., Knight, S., Seetharaman, S., Lakshmanan, N. and Iyer, N. (2011), "Failure Analysis of Transmission Line Towers," *Journal of Performance of Constructed Facilities*, May/June.

SJI (2010), *Standard Specifications, Load Tables, and Weight Tables for Steel Joists and Joist Girders,* 43rd ed., Steel Joist Institute, Myrtle Beach, SC.

Steel Dynamics (2012), "Internal Quality Control Report," Steel Dynamics Corporation, Roanoke, VA.

Yost, J.R., Dinehart, D.W., Gross, S.P., Pote, J. and Gargan, B. (2004) "Strength and Design of Open Web Steel Joists with Crimped-End Web Members," *Journal of Structural Engineering*, Vol. 130, No. 5.

Yost, J.R., Dinehart, D.W., Gross, S.P., Pote, J. and Deeney, J. (2006), "Buckling Strength of Single Angle Compression Members in K-Series Joists," *Engineering Journal,* second quarter.

Experimental Verification of Spliced Buckling Restrained Braces

KENNETH T. TAM, RONALD L. MAYES, DAVID L. MCCORMICK, ANINDYA DUTTA and CRAIG B. GOINGS

ABSTRACT

A critical facility constructed in the 1980s was housed in a building whose original seismic force-resisting system included chevron-braced frames and pre-Northridge earthquake moment frames. In the mid-1990s, a code-based seismic retrofit was designed. This phased retrofit was only partially completed. A more recent seismic evaluation of the building in its partially retrofitted condition revealed major structural deficiencies. Another retrofit was designed using field-spliced buckling restrained braces (BRBs) that allowed the building to remain operational during construction. The paper summarizes the analyses performed for the seismic retrofit and the development, prototype testing and erection of the spliced BRBs. The project testing protocol was compared with current AISC *Seismic Provisions*' testing protocol for BRBs (AISC 341-10), which shows that if properly detailed and fabricated, BRBs used for this retrofit project can have peak and cumulative ductility well in excess of the current AISC testing criteria.

Keywords: seismic retrofit, buckling restrained braces, field-splice details.

INTRODUCTION

A critical facility constructed in the 1980s was housed in a building whose original, seismic force-resisting system includes chevron-braced frames in the long direction and pre-Northridge earthquake moment frames in the short direction. In the mid-1990s, a code-based seismic retrofit was designed. This retrofit, which was scheduled to be completed in phases, was only partially completed after approximately 12 years. A seismic evaluation of the building in 2008 in its partially retrofitted condition revealed major structural deficiencies.

Consequently, a seismic retrofit that consisted of a combination of exterior buttresses with buckling restrained braces (BRBs) and BRB frames at some interior locations was developed. One of the major design constraints was that the facility needed to remain operational during the construction with minimal disruption to existing process utilities.

During the design phase, concern was expressed about the maneuverability of the BRBs in tight spaces inside the building. This resulted in the development of a field-splice detail for the BRBs, which permitted erection of the braces in half-segments. Because splicing of BRBs had not been performed previously, the supplier was required to demonstrate similar performance to the un-spliced BRBs through prototype testing. After the testing, the spliced BRBs were successfully installed and the project was completed with minimal disruption to the operations of the facility.

A summary is presented of the analyses performed for the seismic retrofit and the development, prototype testing and erection of the spliced BRBs. The project testing protocol was compared with current AISC testing protocol for BRBs (AISC 341-10; AISC, 2010), which shows that, if properly detailed and fabricated, BRBs used for this retrofit project can have peak and cumulative ductility well in excess of the current AISC testing requirement.

The subject building is located in South San Francisco, California, and was built circa 1980. It is two stories with a rectangular plan (100 ft by 364 ft). The original building's seismic force-resisting system includes braced frames in the long direction and pre-Northridge earthquake moment frames in the short direction. Figure 1 shows an aerial view of the building. In the mid-1990s, a seismic retrofit was designed to the requirements of the 1991 Uniform Building Code (UBC) with an importance factor of $I = 2.5$. The retrofit primarily involved the addition of braced frames and augmentation of existing moment frame connections at the roof level with haunches. The retrofit, which was progressing in phases during the yearly shutdowns, was only partially (about 60%) completed in 2008 when a new seismic evaluation of the building was commissioned. Major deficiencies in the structure in its partially retrofitted condition were identified. Consequently, a retrofit design was undertaken.

Kenneth T. Tam, S.E., Senior Project Manager, Simpson Gumpertz & Heger, Inc., San Francisco, CA (corresponding). Email: kttam@sgh.com

Ronald L. Mayes, Ph.D., Staff Consultant, Simpson Gumpertz & Heger, Inc., San Francisco, CA. Email: rlmayes@sgh.com

David L. McCormick, S.E., Senior Principal, Simpson Gumpertz & Heger, Inc., San Francisco, CA. Email: dlmccormick@sgh.com

Anindya Dutta, Ph.D., S.E., Senior Project Manager, Simpson Gumpertz & Heger, Inc., San Francisco, CA. Email: adutta@sgh.com

Craig B. Goings, S.E., P.E., Associate Principal, Simpson Gumpertz & Heger, Inc., San Franciso, CA. Email: cbgoings@sgh.com

Many of the spaces are extremely congested with process piping, mechanical ducts and other equipment. Most of the processes could not be altered or taken out of service, even temporarily. Furthermore, two buildings exist adjacent to the north elevation with minimal seismic separation, and a large multilevel pipe rack exists along most of the length at the south elevation. Given the site constraints, a retrofit scheme was developed that utilized exterior steel buttresses on the south elevation, connected to the building with horizontal BRBs at the floor and roof levels, and added BRBs within some of the frame lines that were accessible.

SEISMIC DEFICIENCIES

The partially retrofitted building was analyzed, and the following deficiencies in the seismic load resisting system were identified.

Pre-Northridge Moment Frames

The original lateral system in the transverse direction of the building comprises of W24 (roof) and W30 (second floor) wide flange beams connected to W14 columns with typical pre-Northridge moment connections (WUF) that are susceptible to brittle failure. The frames also have weak panel zones that have capacities well below that required to develop yielding of the beam.

Chevron-Braced Bays

All of the original braced frames and a majority of the retrofitted braced frames have a chevron configuration with beams that were not sized to carry the unbalanced force. This is worsened by the fact that the original braced frames consist of double-tiered chevron frames (two levels of chevron frames per story), where the intermediate beam between story levels consists of W10 wind girts that were oriented with the strong axis in the horizontal position.

Inadequate Brace Connections

All the braces in the original building, as well as a majority of the retrofitted braces and their connections, were not detailed to develop the strength of the braces.

Close Proximity of Adjacent Buildings and Propensity for Pounding

The subject building is located in a congested building complex with at least two buildings spaced closely enough to cause a pounding hazard (see Figure 2).

Other Issues

The building also has a relatively weak, bare-metal roof diaphragm, as well as inadequate collectors and collector connections, in part due to the fact that the retrofit from the 1990s was not completed.

Fig. 1. Aerial view of the facility showing the subject building.

RETROFIT ANALYSIS

A code-type analysis using an *R* factor was not adequate to account for the differing behavior of the various lateral systems that were built in different periods of time. Therefore, a performance-based design approach outlined in ASCE 41-06, *Standard for Seismic Rehabilitation of Existing Buildings* (2006), was followed. The performance objective is to exceed life safety under the BSE-1 level earthquake and collapse prevention under the BSE-2 level earthquake. A nonlinear dynamic analysis using ASCE 41-06 was performed. The analysis was iterative in that it was first required to conceive retrofit concepts and introduce them into the 3D model and then validate through the dynamic analysis that they alter the behavior of the structure in a way that was anticipated. The owner next provides input regarding acceptability with regards to operations and cost. The scheme was then incrementally modified until a cost-effective scheme with little or no temporary or permanent effect on operations was developed.

Retrofit concepts including dampers and conventional braced frames were considered, but it was soon determined that BRBs provided the best protection for the existing braced frames and their connections and limited the drifts in the direction of the moment frames to protect the weak connections and to minimize pounding. Through strategic placement of BRBs—which required replacement of existing chevron braces at some locations—diaphragm strengthening was limited to local areas, and only a limited amount of collector strengthening was required.

As the design progressed, the contractor expressed concerns about maneuverability of the BRBs (approximately 40 ft long) inside the congested building. A field-splice detail for the BRBs, allowing transport of the braces in half-segments, was developed. Because of concerns regarding alignment of the spliced segments, the vendor was required to demonstrate through prototype testing that the spliced braces would perform as well as the non-spliced BRBs. The BRBs were tested at the NCREE facility in Taiwan and the results compared to the analytical model.

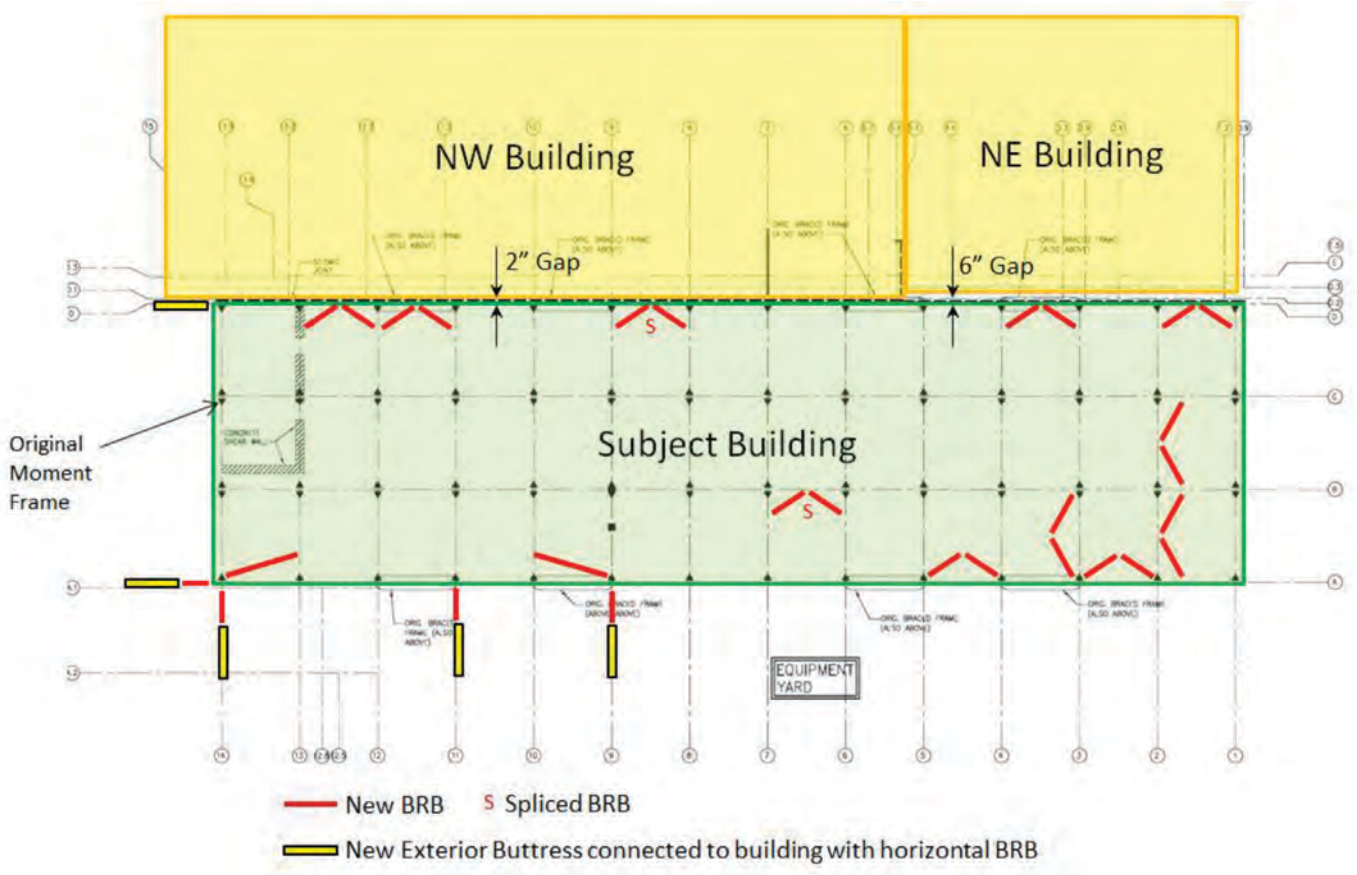

Fig. 2. Plan showing proximity of adjacent buildings.

Table 1. Acceptance Criteria for BRB			
Shaking Level	**Performance Goal**	**Average of 7 Time Histories**	**Maximum of 7 Time Histories**
BSE-1	Life safety	$8\Delta_{by}$	$12\Delta_{by}$
BSE-2	Collapse prevention	$12\Delta_{by}$	$18\Delta_{by}$

Ground Motion for Nonlinear Analysis

A suite of seven ground motions was used for the nonlinear time-history analyses. These ground motions were scaled to a site-specific spectra generated using the next-generation attenuation (NGA) relationships. As the soil profile changes dramatically under the building, the worst-case ground motions associated with a firm and soft soil site were used.

Nonlinear Analysis Model

A nonlinear finite element model of the lateral-load systems of the building was created using the analysis program CSI Perform. Existing double-angle and tube steel braces were modeled using backbone parameters from ASCE 41-06. One of the most important criteria for modeling the braces was to capture the behavior of weak connections. Where strength of the connection governed, a drastic drop in strength was incorporated into the model. The brace was considered ineffective after the connection fails. Similar modeling was performed to recognize substantial loss of strength when the braces buckled. The moment frames were modeled with a nonlinear panel zone spring to capture the effects of the weak panel zone.

The effects of foundation flexibility were included into the model through the use of nonlinear elastic springs representing the passive and frictional resistance of the footings against the supporting soil. Nonlinear gap elements with compression only stiffness were used to capture foundation uplift. The upper- and lower-bound analysis of the structure using 150% and 67% of the soil stiffness to capture the variability in the behavior were used in accordance with the requirements of ASCE 41-06.

The BRBs were modeled with a component consisting of stiff end zones and a yielding core. The backbone parameters are shown in Figure 3. These parameters were based on prior testing performed by the BRB manufacturer. Because there are no criteria for checking BRBs in ASCE 41-06, strains in the individual BRBs were checked to the criteria listed in Table 1. These criteria were derived based on a review of existing test data from the BRB manufacturer. It can be seen from Table 1 that separate criteria for the average of the seven time histories and maximum from any single event were used. Both criteria needed to be satisfied.

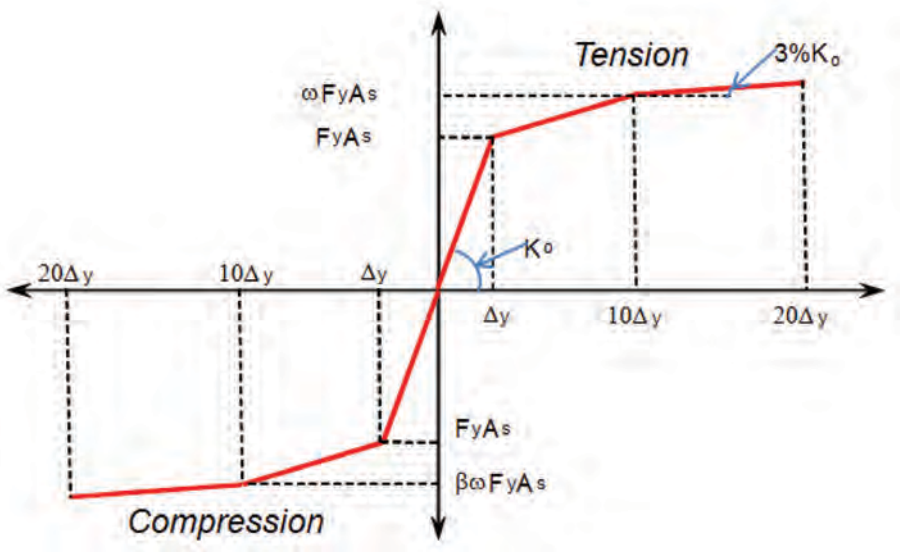

Fig. 3. Backbone properties of buckling restrained braces.

DETAILS OF THE SPLICED BRB

As indicated previously, a spliced BRB was developed to help with the maneuverability of the BRB members within congested areas. The spliced BRB consists of two BRB segments; each segment alone is similar to a standard BRB consisting of a yielding core, transition zones and nonyielding end zones (see Figure 4). The concept behind the spliced BRB is that the splice zone is designed to remain elastic (similar to typical end zones). The core at the splice zone has a cross-sectional area much larger than the yielding core, and the splice of the casing was designed to have flexural stiffness exceeding the casing along the remaining length of the BRB. Several conceptual splices were assessed, including welded and bolted options (see Figure 5).

The welded option was chosen based on the stability of the cruciform shape as well as the constructability of the detail. The final detail consists of cruciform cores at the splice zone, which are connected with full-penetration welds. The outer casing was connected with plates welded to each other and to the casing with fillet welds. The final detail of the splice is shown in Figure 6.

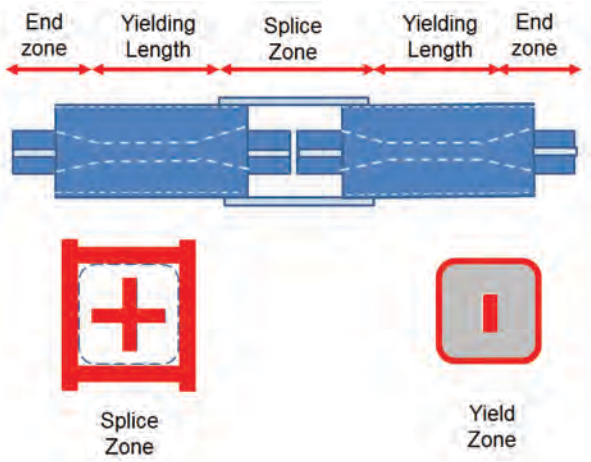

Fig. 4. Conceptual sketch for spliced BRB.

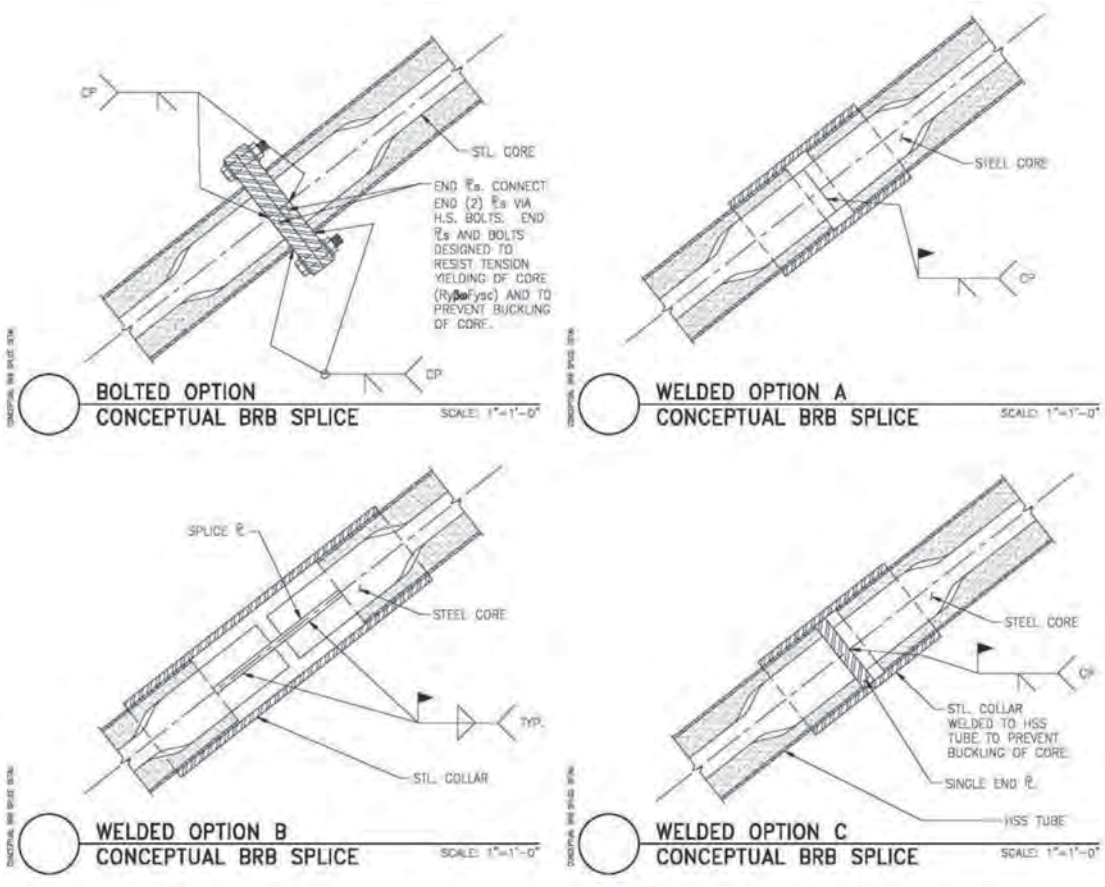

Fig. 5. Conceptual studies of splice options.

Note that the yielding core of the spliced BRB is shorter than a standard BRB of the same length because there are essentially four end and transition zones, doubling that of a standard BRB. The analysis model included this to capture the correct load distribution within the structure as well as the ductility demand on the cores. Locations of the spliced BRB within the structure were closely coordinated with the contractor during the design phase. Many site visits and some inspection openings were made during the design phase to work out the locations of the spliced and nonspliced BRBs. Subsequently, many iterations of the model were created.

BRB PROTOTYPE TESTING

Because spliced BRBs have not been implemented before, prototype specimens were fabricated for testing. The objectives of the testing program were as follows:

- To validate that the spliced BRB is feasible and the behavior is as anticipated.
- To determine any potential obstacles related to the erection of the spliced BRBs.
- To ensure that the two halves of the spliced BRB can be properly aligned given the congested field conditions.

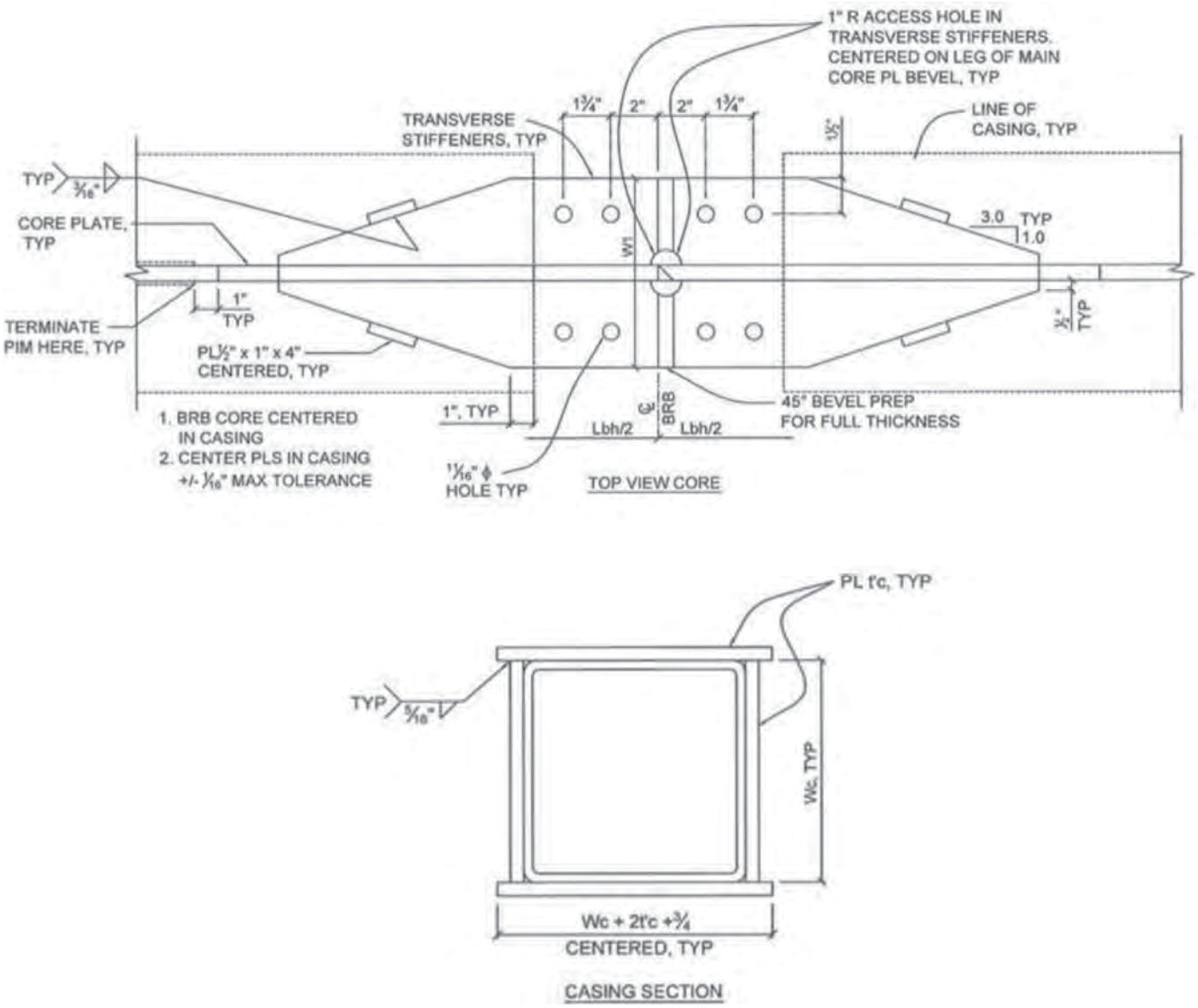

Fig. 6. Final details of splice.

Table 2. Summary of BRB Test Specimens							
Number	ID	Length, L_b (ft)	Yield Length, L_y (in.)	Casing Size	End Connections	P_{ysc} (kips)	Spliced
1	1901A1	12	86.2	HSS10×¼	Pin-end	250	No
2	1901A2	12	86.2	HSS10×¼	Pin-end	250	No
3	1902A1	21	125.6	HSS10×10×½	Bolted-end	230	Yes
4	1902A2	21	125.6	HSS10×10×½	Bolted-end	230	Yes
5	1903A	31	236.7	HSS10×10×½	Bolted-end	250	Yes
6	1904A	31	268.5	HSS10×10×½	Bolted-end	250	No

- To develop quality assurance requirements for splicing BRBs in the field.

Additionally, testing on three unspliced BRBs was performed to study the effects of the following:

- Performance of pin-ended BRBs with casing fabricated with circular HSS section. The pin-ended BRB was developed to be a high-performance brace that includes some of the special detailing not used in previous versions. Thus, testing was performed to validate the performance.

- Performance of relatively long and slender BRBs. Note that this was also intended to be a control, or comparison, to the spliced version.

DESCRIPTION OF PROTOTYPE SPECIMENS

A total of six specimens were tested. The yielding cores of the BRB were fabricated with ASTM A36 plate stock with the following properties: F_y = 41.9 ksi and F_u = 71.6 ksi based on average of two coupon tests using the 0.02% offset method. The gusset plates were made with ASTM A572 Grade 50 steel.

Three specimens were spliced. Two of the spliced specimens were 21 ft long and the third was 31 ft long. Three specimens were not spliced: two 12-ft-long pin-ended specimens, and one 31-ft-long bolted-end specimen. Properties of the test specimens are summarized in Table 2.

DESCRIPTION OF FABRICATION

The prototypes were fabricated at the manufacturing facility in Utah. The construction of the spliced specimens (specimens 3, 4 and 5) was observed to develop procedures to perform the splices and to identify potential problems during construction.

Method of Alignment

One of the objectives of the prototype testing was to determine whether the two halves could be properly aligned in the field. Alignment plates to align the cruciform cores were proposed (see Figures 7 and 8). The alignment plates were removed in stages as the cores were welded together. To align the casing, two pairs of steel angles were clamped onto the steel casings. A small amount of welding was used to connect the angles with the casing (see Figure 9). The alignment angles were removed in stages as the casing splice plates were welded. Figure 10 shows the finished spliced condition.

The original intent was to make the splice in the horizontal position (on the ground) prior to lifting the BRB into the final locations. However, it was determined that this required substantially more floor area than is available in the building. During one of our visits to the site during the design phase, the contractor requested the option of lifting each half of the BRBs into the inclined position (final position of the brace) prior to performing the splice. In order to replicate the actual condition of the site, one of the specimens was spliced in the inclined location (see Figure 11). As shown in Figure 11, the prototype was supported at the splice point by a crane. In the field, this would be accomplished by a combination of chains and come-alongs. The alignment, welding of the cores and welding of the casing plates of the specimen were performed in this position.

Effects of Welding of the Core

The cores were spliced with prequalified, full-penetration welds. The weld of the core splice was treated as a demand-critical weld with associated quality assurance (ultrasonic testing, magnetic particle testing) even though no yielding is expected to occur at this location. The maximum thickness of the core plates was 1 in. Some amount of distortion was observed, primarily due to the heat generated during the welding process. As a result, some out-of-straightness

was measured after the cores were welded. It was noted that the sequence of laying down the weld beads was an important aspect of controlling the amount of distortion (i.e., the welder needed to alternate the weld placed on each leg of the cruciform core). Additionally, in order to prevent initial stressing of the core due to heating and subsequent cooling of the core, tightening of bolts at the end connections was permitted only after the splice was complete and adequate time passed for cooling of the welded zone.

Tolerance

As discussed earlier, the cores were aligned using alignment plates. Following this procedure, the out-of-plane offset tolerance of the cores was limited to 1/16 in. The out-of-straightness tolerance (both in-plane of the core and out-of-plane of the core, see Figure 12) was initially set to be 1/16 in. over the length of the completed brace. This was measured prior to welding of the cores. As part of the field quality assurance, a second measurement was required after the cores were welded. For this measurement, the tolerance was relaxed to 1/8 in. over the length of the brace. It was noted that during the welding of the splice of specimen 5, the out-of-straightness tolerance was exceeded in the out-of-plane direction. The measured out-of-straightness in the specimen was 1/4 in. over the length of the brace. This was likely due to sequence of laying down the weld beads. In lieu of attempting to straighten this specimen, it was decided to test the specimen to study the effect on performance of some

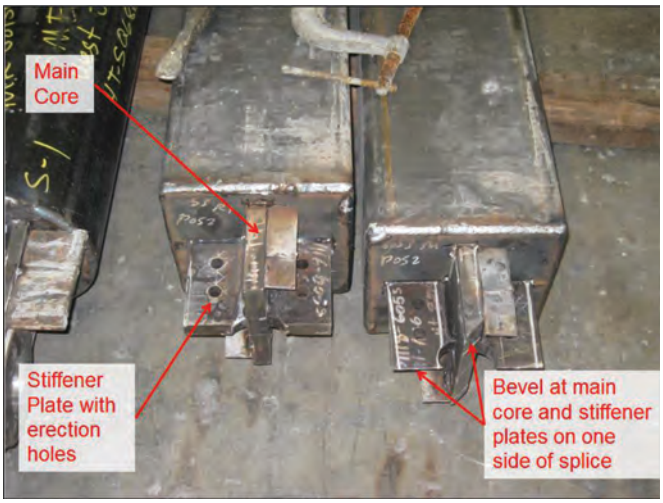

Fig. 7. Core at splice location.

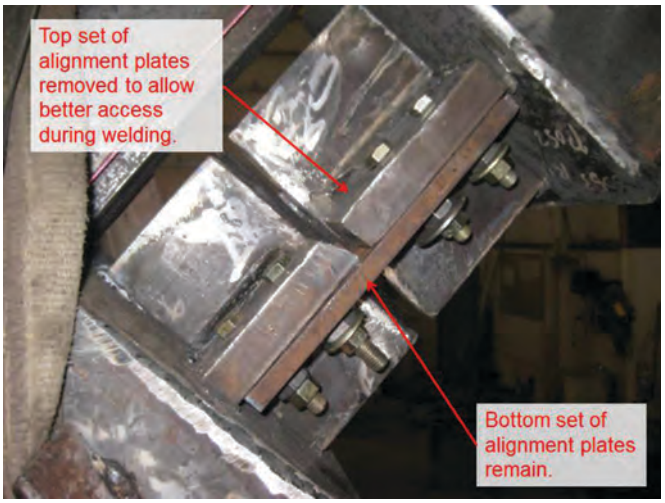

Fig. 8. Alignment plates at core at splice.

Fig. 9. Alignment aid for casing.

Fig. 10. Finished splice.

Fig. 11. Prototype spliced in inclined position.

Table 3. Measured Alignment on Test Specimens with Spliced BRBs					
		Alignment before Welding Core + Stiffener (in.)		Alignment after Welding Core + Stiffener but before Welding Casing Plates (in.)	
Number	ID	In-Plane	Out-of-Plane	In-Plane	Out-of-Plane
3	1902A1	<1/16	<1/16	<1/16	<1/8
4	1902A2	<1/16	<1/16	<1/8	<1/8
5	1903A	<1/16	<1/16	<1/8	<1/4

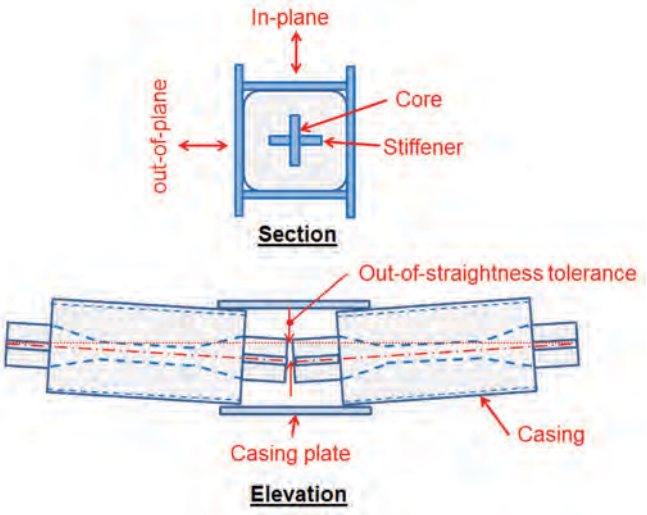

Fig. 12. Out-of-straightness tolerance.

out-of-straightness in the splice. Table 3 summarizes the tolerance measured from the spliced specimens.

BRB TESTING

The tests were conducted using the Multi-Axial Testing System (MATS) at the National Center for Research on Earthquake Engineering (NCREE), Taipei, Taiwan (Tsai et al., 2010a, 2010b). The MATS platen is capable of imposing displacements in all six degrees of freedom. For the tests, longitudinal and transverse displacements were imposed simultaneously to capture the axial and rotational demands on the specimen. One end of the specimen was attached to a concrete strong wall, while the other was attached to the MATS platen where the deformations were imposed on the specimen via horizontal and vertical actuators. Figures 13 and 14 show the test setup for the 21-ft-long braces (specimens 3 and 4). Four displacement transducers (D1 to D4 shown in Figure 13) measure the axial deformations of the brace specimen (D1 and D2) and gusset brackets (D3 and D4). The brace axial deformation, Δ_b, is taken as the average

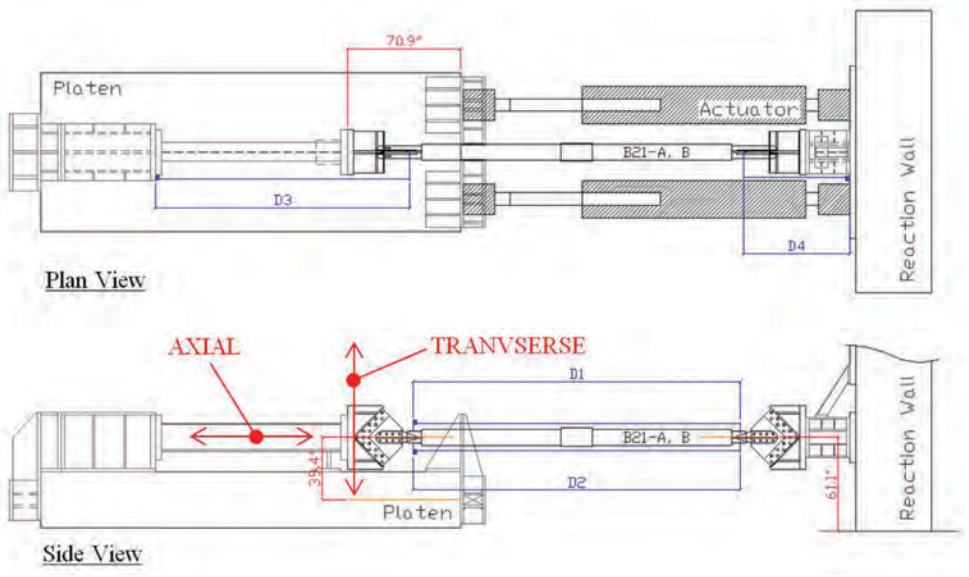

Fig. 13. Test setup.

of the displacement measured by displacement transducers D1 and D2. Transducers D3 and D4 measure the deformations of the gussets, wall bracket, platen brackets and fixtures, as well as deformations due to bolt slip. Longitudinal and transverse displacements of the platen were also recorded. The force measured by the load cell in each actuator that drove the platen was recorded. The test setup for the other braces is similar.

The BRBs were connected to gusset plates similar to those in actual construction. To reduce the cost of the testing program, as well as shorten the time between each set of tests, the gusset plates for each type of end connection were reused; that is, the same gussets for pin-end were used for both specimens 1 and 2, and the gussets for bolt-end were used for specimens 3 through 6. The gusset plates were bolted to reaction blocks, which were in turn anchored to the strong wall and platen.

DISPLACEMENT HISTORY

Subassemblage tests were performed for all six specimens. The test protocol was selected to capture the expected ductility demand of the yielding section of the steel core, obtained from the nonlinear dynamic analysis. The test protocol is defined in terms of multiples of yield displacement of the core, Δ_{by}, defined as $P_{syc}L_{ysc}/A_{sc}E$.

The parameter Δ_{by} was chosen primarily because the yielding and nonyielding length of the BRB was explicitly modeled, and the interest is in the actual ductility demand on the yielding portion of the core. The actual displacement imposed on the specimen was increased to capture the following: (1) bolt slip at the connections; (2) elastic deformation of the nonyielding section of the BRB, including the splice; and (3) elastic deformations of the gusset plates and connection fixtures. During the tests, the deformation of the platen was adjusted to ensure the amount of deformation due to bolt slip and elastic deformation of the connection fixtures were properly measured. In most cases, the actual imposed deformations on the specimen exceed that required by the protocol because the connection fixtures, bolts and so on did not move as much as anticipated.

The AISC *Seismic Provisions* (AISC 341-10) require the specimen to be tested to $2\Delta_{bm}$, where Δ_{bm} is the brace deformation corresponding to design story drift or 1% story drift, whichever is larger. Specimens 1 and 2 represent the pin-end braces connecting the building to exterior buttresses. Unlike typical braced frames that are installed between different floors of a building, these braces are horizontal, and the brace deformation is not dependent on interstory drift; rather, it is dependent on the relative displacement between the building and the exterior buttresses. Therefore, the code requirement of minimum 1% interstory drift is not relevant in this case. For these braces, the maximum deformation of the braces under BSE-2 from our computer model was used to establish Δ_{bm}.

For the braces that are installed between floors, $2\Delta_{bm}$ (governed by the code minimum of Δ_{bm} = 1%) equates to approximately $14\Delta_{by}$ for the 21-ft specimens (specimens 3 and 4), $10\Delta_{by}$ for the 31-ft spliced specimen (specimen 5) and $9\Delta_{by}$ for the 31-ft unspliced specimen (specimen 6). The differences are due to different geometry of BRBs and different yielding length of the core as a percentage of the overall length for spliced and unspliced BRBs. Studies by Fahnestock, Sause and Ricles (2006), Mayes et al. (2004), and Sabelli, Mahin and Chang (2003) have indicated that the current protocol shown in AISC 341-10 for qualification of BRBs may not be adequate to capture maximum ductility demands on the BRBs, especially under maximum

Fig. 14. Test setup.

Table 4. Project Test Protocol		
Cumulative Number of Cycles	**Number of Cycles at the Specified Deformation**	**Longitudinal Loading in Terms of Multiples of First Significant Yield of Steel Core (Δ_{by})**
2	2	$1\Delta_{by}$
8	6	$2\Delta_{by}$
10	2	$3\Delta_{by}$
12	2	$6\Delta_{by}$
17	5	$2\Delta_{by}$
19	2	$9\Delta_{by}$
24	5	$2\Delta_{by}$
26	2	$13\Delta_{by}$
31	5	$2\Delta_{by}$
33	2	$15\Delta_{by}$
38	5	$2\Delta_{by}$
39	1	$18\Delta_{by}$
44	5	$2\Delta_{by}$
45	1	$21\Delta_{by}$
50	5	$2\Delta_{by}$

considered earthquakes (BSE-2 level earthquake per ASCE-41-06) for low- to mid-rise buildings. Many of the existing published tests have been limited to AISC requirements for maximum ductility. In order to study whether the BRBs can accommodate anticipated deformation under BSE-2, the braces were tested to at least $21\Delta_{by}$.

In addition, results from the nonlinear time-history analyses showed that cycles of large excursions were interspersed by cycles of relatively small displacements. For this reason, the project protocol was designed with five to six cycles of small deformations ($2\Delta_{by}$) in between two cycles of large deformations ranging from $3\Delta_{by}$ to $21\Delta_{by}$. See Table 4 for the project test protocol.

To capture concurrent axial and rotational demands on the brace, transverse displacements were applied simultaneously to the axial displacements to meet the AISC 341-10 "subassemblage" test requirements. As discussed earlier, specimens 1 and 2 are for pin-end braces connecting the building and exterior buttresses; thus, brace rotation demand is from the building horizontal displacement perpendicular to the axis of the braces. The transverse displacements were 30% of those required by axial demand. For the remaining specimens, the transverse displacements were based on the geometry of the braced frames. That is, the 21-ft BRBs (specimens 3 and 4) are intended for frames in chevron configuration with slope of 1:1 (horizontal to vertical); thus, the transverse displacements were equal to the longitudinal displacements. The 31-ft-long BRBs (specimens 5 and 6) are intended to be in single diagonal configuration with slope of 2:1; thus, the transverse displacements were 60% of the longitudinal displacements. The range of vertical displacement of the equipment was limited to ±2.5 in. and cannot accommodate both maximum positive and maximum negative transverse displacements (which exceed 4 in. at larger cycles) for the longer braces. An initial offset of 2 in. was introduced to the platen table, giving it a range of +0.5 in. and −4.5 in. to allow the required maximum transverse displacement in negative direction.

Figure 15 (page 34) shows the project testing protocol for the 21-ft-long BRBs, and Figure 16 (page 35) shows the testing protocol for the minimum criteria outlined in AISC 341-10. The total cumulative ductility demand for the project test protocol is in excess of $500\Delta_{by}$, which substantially exceeds the $200\Delta_{by}$ that is currently required by AISC 341-10. The project testing criteria are much more demanding than the AISC testing protocol in terms of number of cycles and cumulative and peak ductility.

Subsequent to the project test protocol, all specimens were tested to failure with either a high amplitude protocol or increasing amplitude protocol.

For specimens 1 and 2, the failure test was based on incrementally increasing the amplitude at each cycle until failure (see Table 5). For specimens 3, 4 and 5, we elected to study the effect of a potential aftershock with lower amplitude but a larger number of cycles. In these failure tests, the amplitude of the largest cycle was limited to $15\Delta_{by}$ and repeated until the specimen failed (see Table 6).

Table 5. High-Amplitude Protocol (Specimens 1 and 2)		
Cumulative Number of Cycles (including main test)	**Number of Cycles at the Specified Deformation**	**Increasing Deformation Corresponding to Multiples of First Significant Yield of Steel Core (Δ_{by})**
51	2	$24\Delta_{by}$
53	2	$27\Delta_{by}$
55	2	$30\Delta_{by}$
57	2	$33\Delta_{by}$
59	2	$36\Delta_{by}$
61	2	$39\Delta_{by}$

Table 6. High-Cycle Protocol (Specimens 3, 4 and 5)		
Cumulative Number of Cycles (including main test)	**Number of Cycles at the Specified Deformation**	**Deformation Corresponding to Multiples of First Significant Yield of Steel Core (Δ_{by})**
51	2	$3\Delta_{by}$
54	3	$2\Delta_{by}$
56	2	$6\Delta_{by}$
59	3	$2\Delta_{by}$
61	2	$9\Delta_{by}$
Until failure	Until failure	$15\Delta_{by}$

EXPERIMENTAL RESULTS

Specimens 1 through 5 passed the project protocol test sequence without failure. The behavior of the braces was stable and repeatable at each cycle. The steel core projection, where it exits the casing, did not show any unusual deleterious effects from the combined axial and flexural strains. No visible lateral displacement was observed for any of the specimens, including those with splices.

During the high-amplitude protocol tests, the steel cores for specimens 1 and 2 fractured in tension during the first and second cycles of the high-amplitude test, respectively. During the high-cycle protocol testing, steel cores of specimens 3, 4 and 5 fractured in tension during the seventh, third and third cycles at $15\Delta_{by}$, respectively.

Specimen 6 exhibited gusset bending and buckling during the compression cycle at $21\Delta_{by}$ during the project testing protocol. At this cycle, the brace had been subjected to cumulative inelastic deformation in excess of $730\Delta_{by}$, based on actual measured deformation. It is important to note the same gussets had been used for the previous three specimens.

For bolt-ended BRBs (specimens 3 through 6), bolt slip was observed at cycles with amplitudes exceeding $9\Delta_{by}$. The slip-critical bolts were sized for service-level loads. After the tests, we examined the bolt holes and did not observe any evidence of deformation at bolt holes.

The summary of test results, including effects of test protocol and subsequent high-amplitude or high-cycle protocol tests, for each of the six specimens is shown in Table 7.

Comparing maximum longitudinal deformation between specimens 5 and 6, the brace with splice (specimen 5) performs as well as the brace without splice (specimen 6) in terms of maximum ductility achieved in the yield length, even though the spliced specimen has a built-in imperfection—that is, out-of-straightness of ¼ in. over the length of the brace. However, because the yield length of the spliced specimen is shorter than nonspliced specimen, the corresponding drift is also lower. Nonetheless, all the spliced specimens achieved at least 3.4% interstory drift, which is well in excess of 2% drift required by AISC 341-10 and the calculated demand from the nonlinear time-history analyses.

Table 8 shows the tension strength adjustment factor (ω), and compression strength adjustment factor (β) for the specimens at peak response as well as at 2% story drift obtained from the tests.

The ω values are generally slightly lower than the value used in the nonlinear time-history analysis, whereas the β values are generally higher than that used in the analysis, especially for the bolted end specimens (specimens 3 through 6). Note that all β values are still within the AISC 341-10 limit of 1.3 at two times the design story drift, or 2%.

The plots showing the applied load versus brace

Table 7. Summary of Test Results						
Specimen Number	**ID**	**Maximum Longitudinal Deformation for All Cycles**	**Corresponding Interstory Drift**	**Number of Cycles at High Amplitude**	**Number of Cycles at $15\Delta_{by}$**	**Cumulative Inelastic Deformation for All Cycles**
1	1901A1	$22\Delta_{by}$	NA[1]	1	NA	$750\Delta_{by}$
2	1901A2	$24\Delta_{by}$	NA[1]	2	NA	$947\Delta_{by}$
3	1902A1	$23\Delta_{by}$	3.4%	NA	7	$1515\Delta_{by}$
4	1902A2	$23\Delta_{by}$	3.4%	NA	3	$1472\Delta_{by}$
5	1903A	$22\Delta_{by}$	5.1%	NA	3	$1141\Delta_{by}$
6	1904A	$22\Delta_{by}$	5.8%	NA	0[2]	$736\Delta_{by}$

Notes:
1. Horizontal braces (specimens 1 and 2) are not related to interstory drift.
2. Specimen 6 exhibited gusset bending and buckling during the last compression cycle of the project protocol.

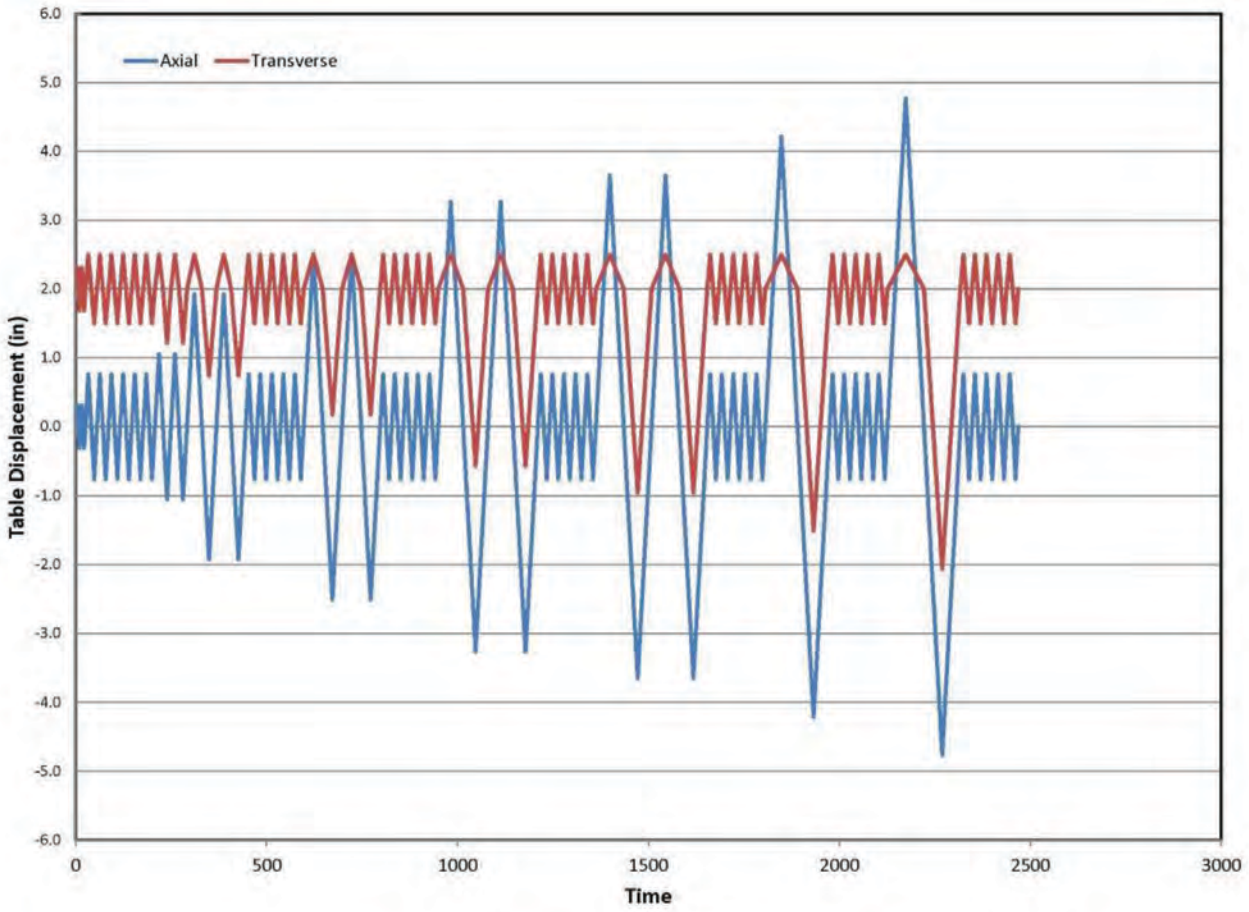

Fig. 15. Project test protocol.

Table 8. Summary of β and ω				
Specimen Number	Maximum Response Quantities for All Cycles		Maximum Response Quantities for 2% Story Drift	
	β	ω	β	ω
1	1.16	1.58	NA	NA
2	1.16	1.57	NA	NA
3	1.32	1.53	1.27	1.36
4	1.34	1.51	1.25	1.37
5	1.54	1.57	1.19	1.29
6	1.55	1.73	1.27	1.21

deformation for the specimens are shown in Figures 17 through 22. The dashed line represents the hysteresis behavior inputted into the computer model. As shown, at higher ductility levels, the computer model overestimates the tensile force and underestimates the compression force in the BRB (especially for the specimens with bolted ends) due to the ω and β values used. The computer model underestimates the hysteretic damping at higher ductility levels.

Review of the analysis results and computer models revealed that only a few BRBs in the project reached ductility levels in excess of $18\Delta_{by}$ under BSE-2 level seismic ground motions. The elongations for the majority of the

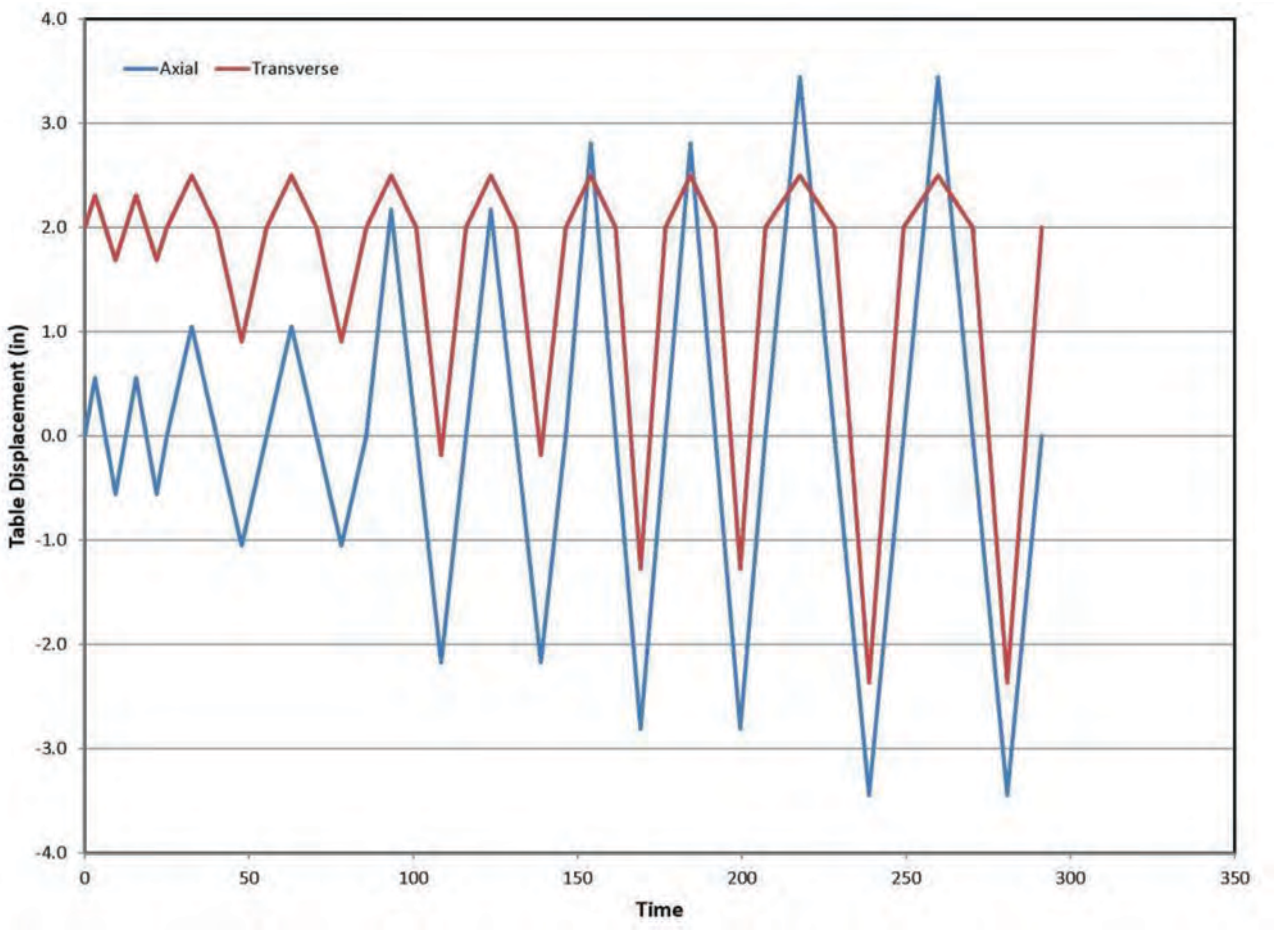

Fig. 16. AISC 341-10 test protocol.

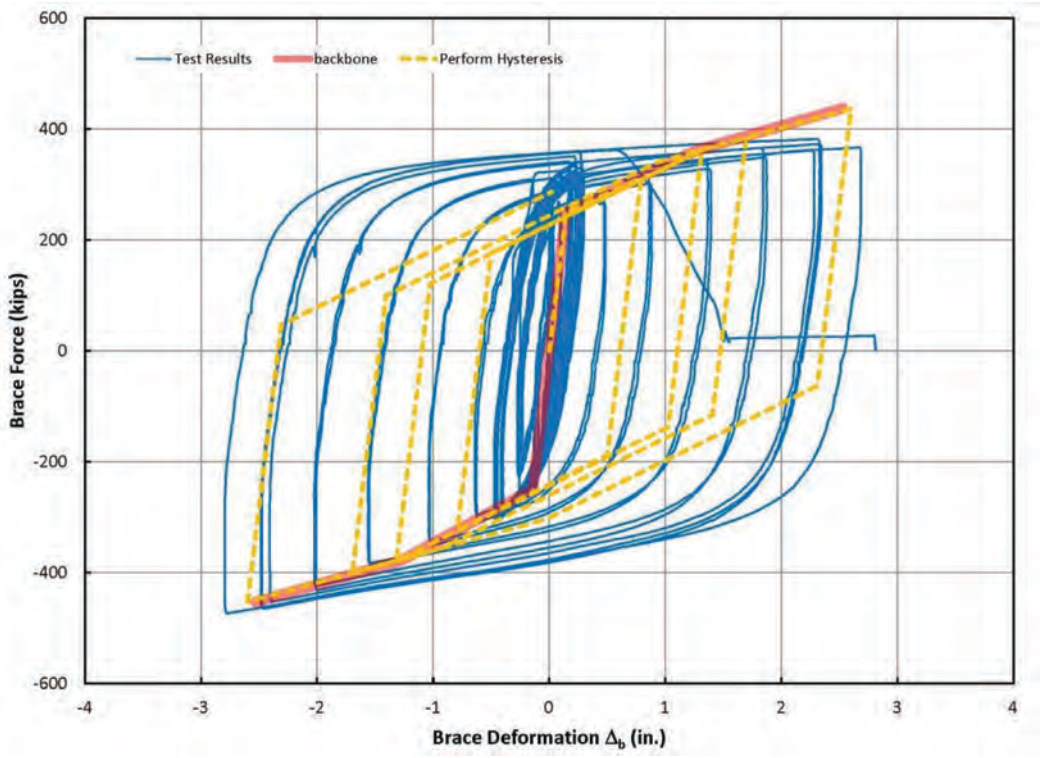

Fig. 17. Test results for specimen 1 (12-ft pinned end).

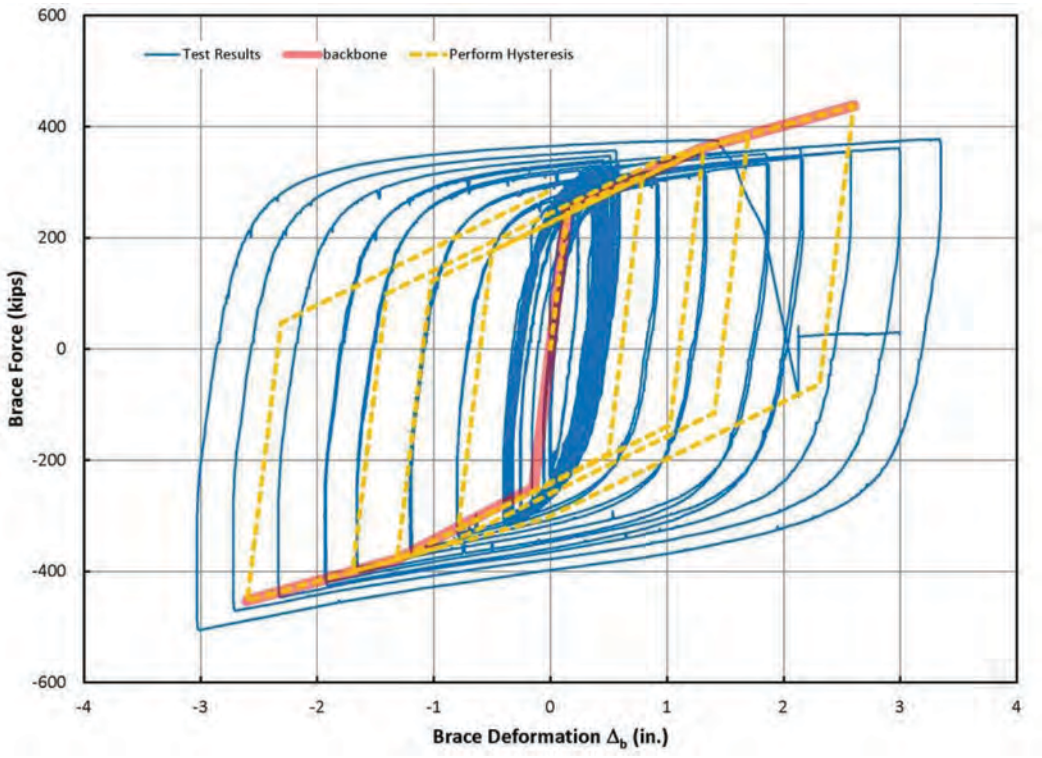

Fig. 18. Test results for specimen 2 (12-ft pinned end).

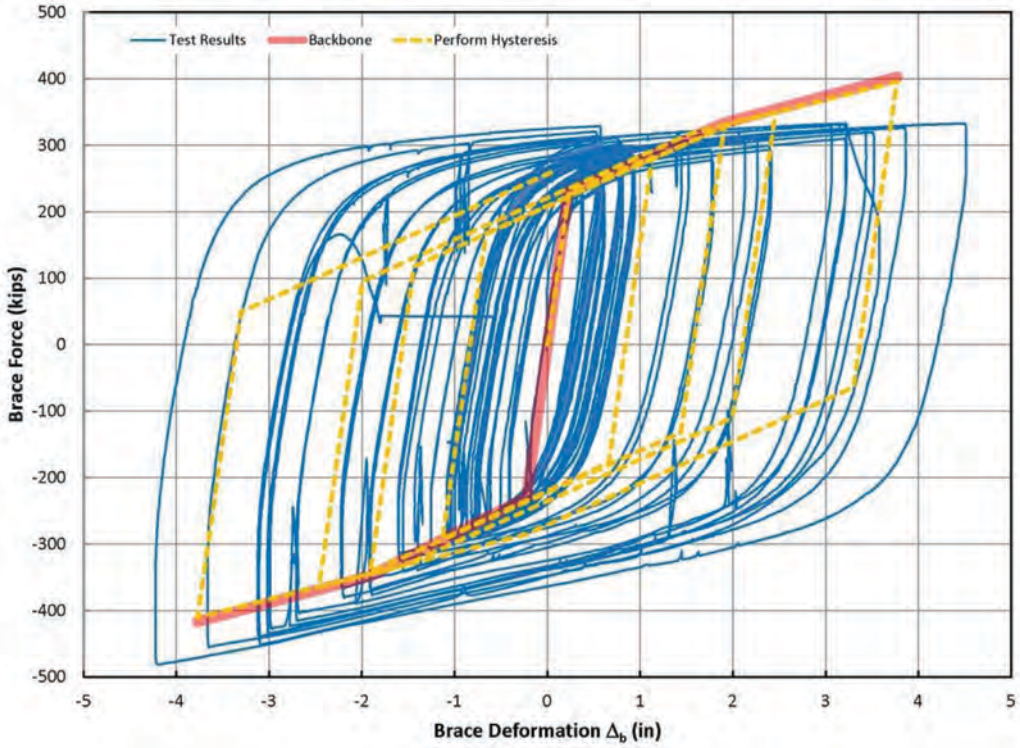

Fig. 19. Test results for specimen 3 (21-ft spliced).

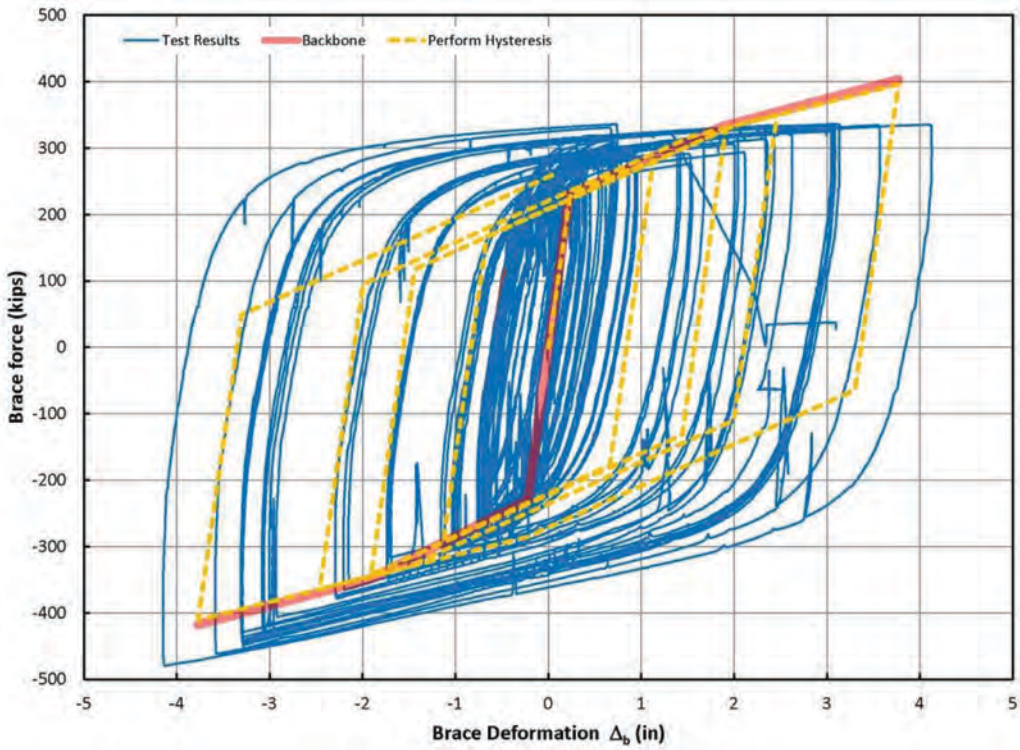

Fig. 20. Test results for specimen 4 (21-ft spliced).

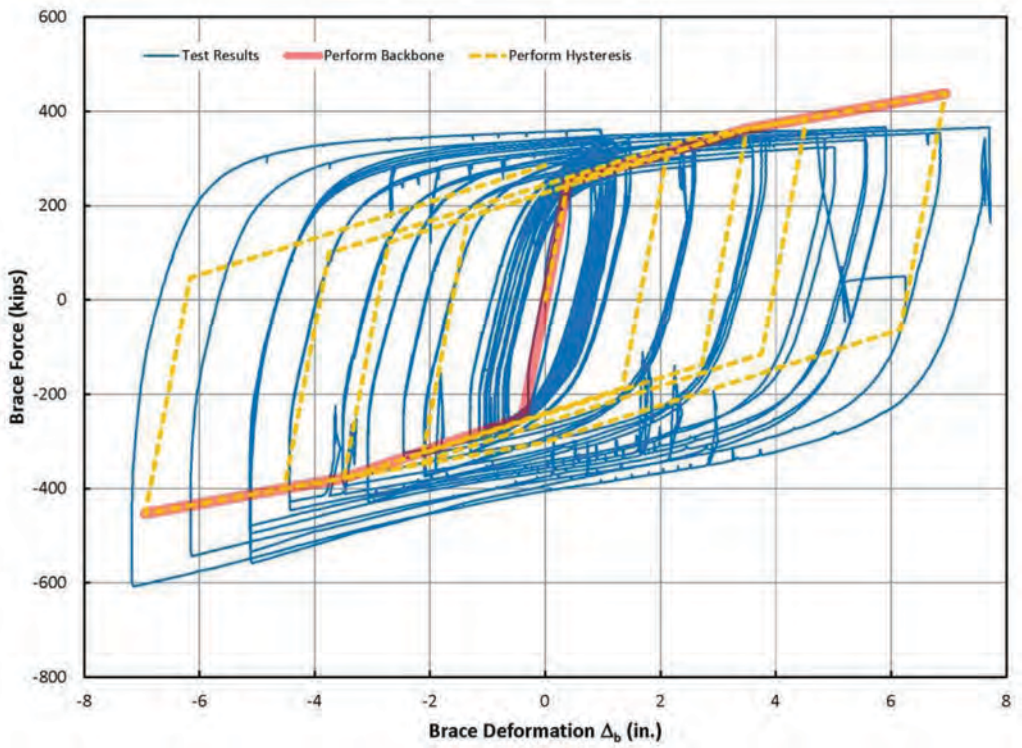

Fig. 21. Test results for specimen 5 (31-ft spliced).

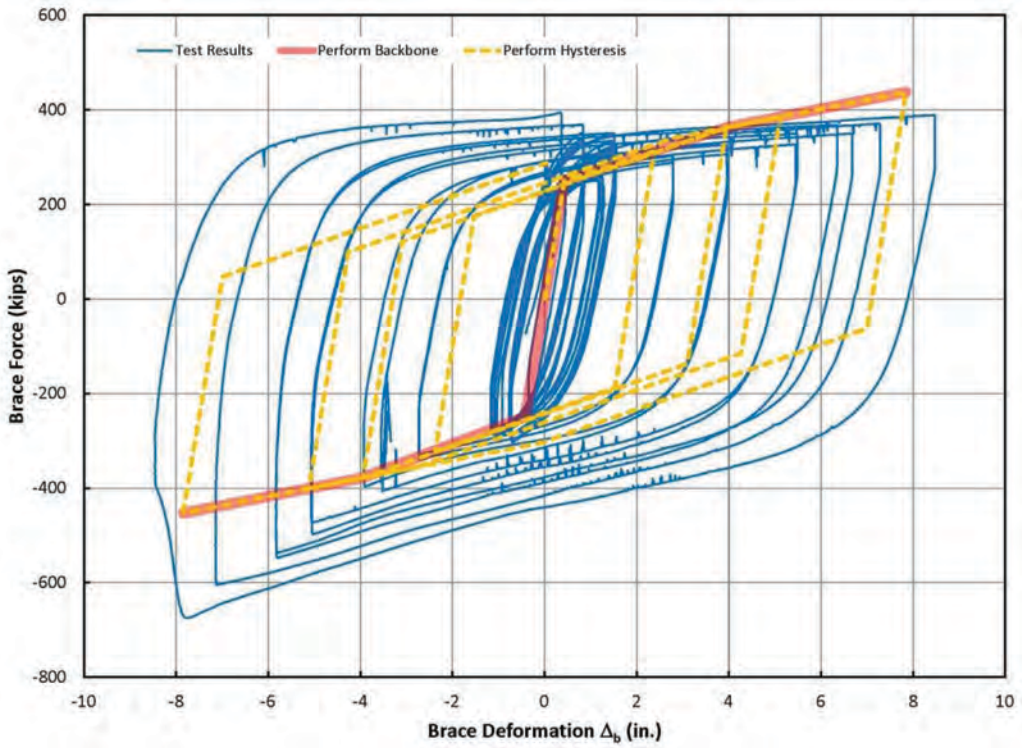

Fig. 22. Test results for specimen 6 (31-ft nonspliced).

BRBs remained within $9\Delta_{by.}$ Figures 23 through 26 shows the test results for specimens 3 through 6 within brace elongations at $9\Delta_{by.}$ At this ductility level, the computer model matches the tested BRB behavior very well.

Based on the results, the following conclusions and observations can be made:

- Plots showing the applied load versus brace deformations show stable, repeatable behavior.
- For all cycles within 2% of the interstory drift, the maximum compression force to maximum tension force (β) did not exceed 1.3.
- At larger drifts (i.e., ductility level), the maximum compression force to maximum tension force (β) is higher than 1.3. Further study is required to determine the cause.
- The cumulative inelastic axial deformation achieved by all specimens was significantly greater than the $200\Delta_{by}$ required by AISC 341-10.

CONSTRUCTION

The retrofit of the building started in early 2011. Congestion during construction was a major challenge. Figure 27 shows one such condition, where there were only inches between the BRB and the adjacent process lines. Nonetheless, the spliced BRBs were successfully installed without significant issue. The actual, measured, out-of-plane and out-of-straightness for each of the BRBs was well below the allowed tolerance. Aside from the scheduled 2-week shutdown period, the building was in full operation during the entire construction period.

CONCLUSIONS

Buckling restrained brace (BRB) frames have gained increasing acceptance in the structural engineering profession for seismic load-resisting systems of new and retrofit construction. A spliced BRB was developed where site conditions would not allow a standard BRB to be installed. The testing program and subsequent construction showed that the spliced BRB can be used when needed. The performance of

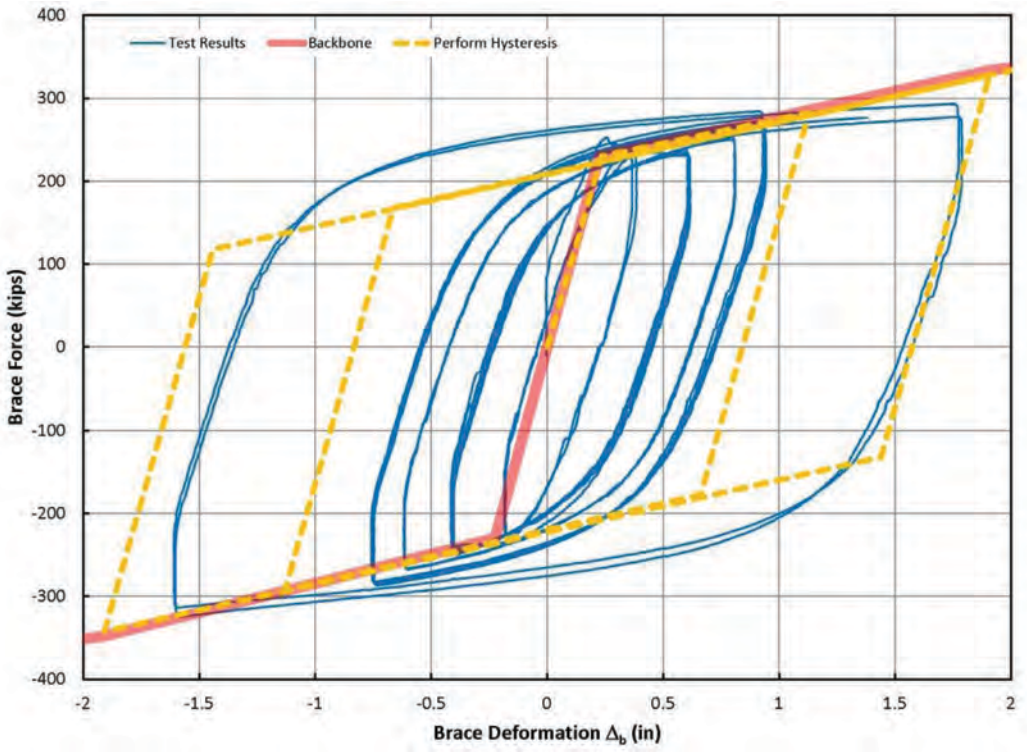

Fig. 23. Test results for specimen 3 within $9\Delta_{by}$.

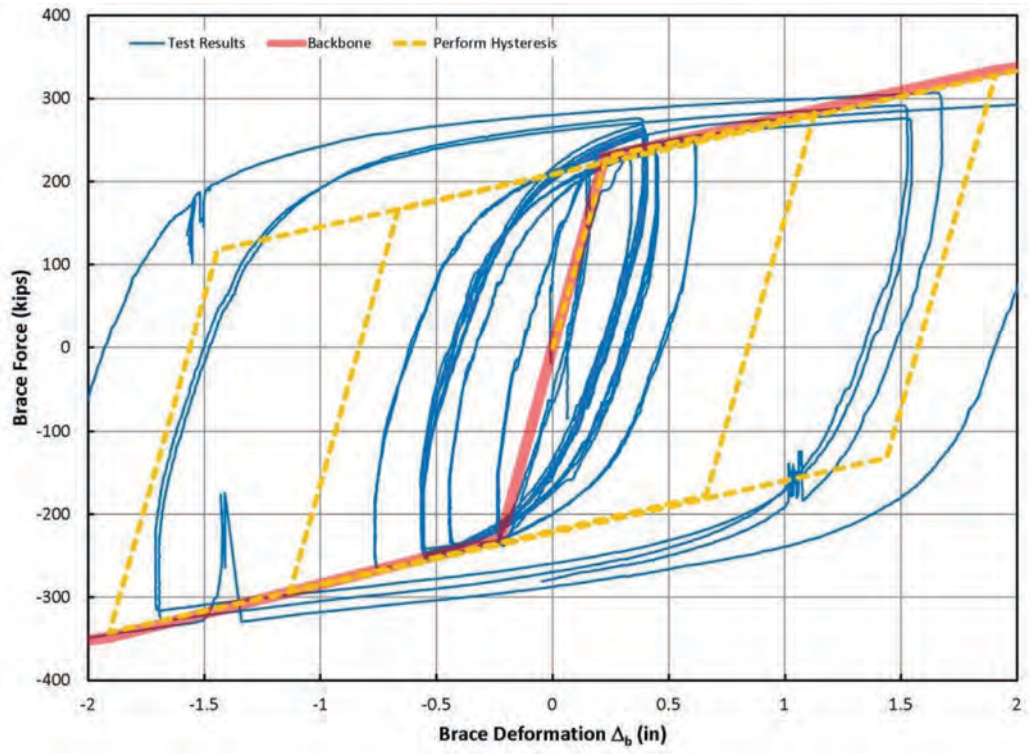

Fig. 24. Test results for specimen 4 within $9\Delta_{by}$.

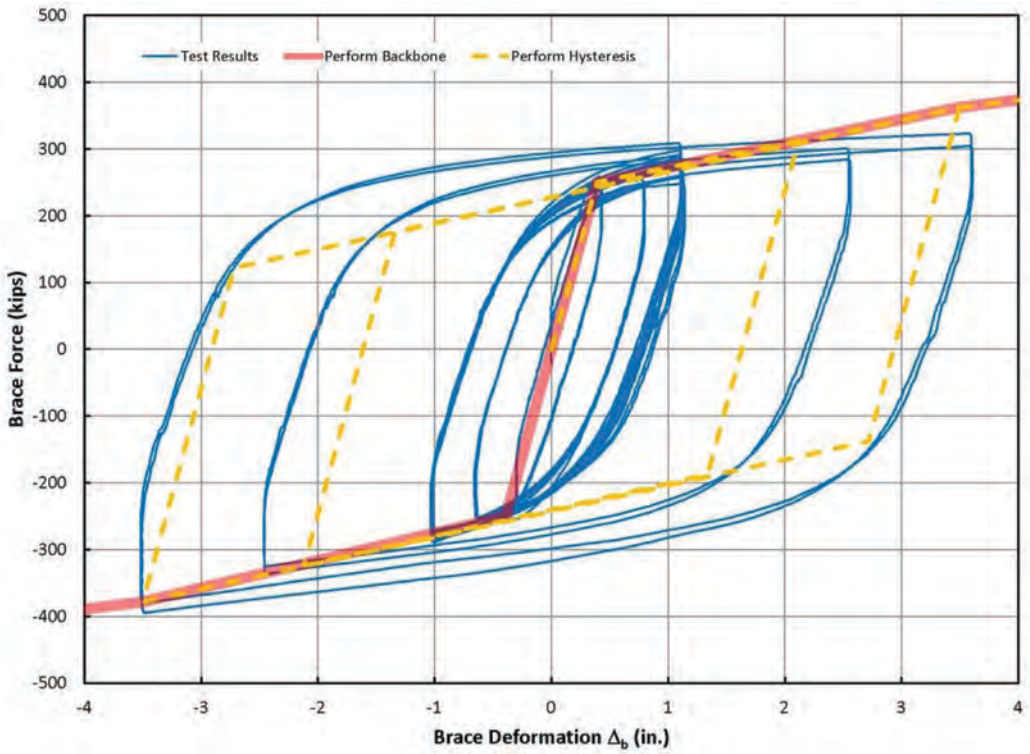

Fig. 25. Test results for specimen 5 within $9\Delta_{by}$.

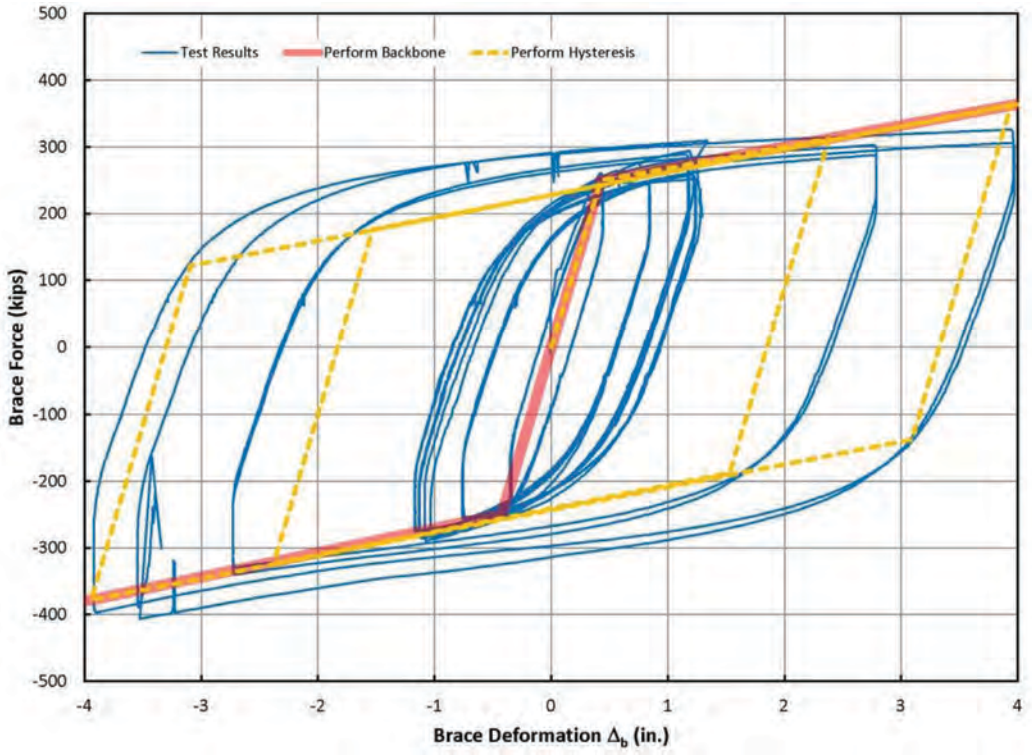

Fig. 26. Test results for specimen 6 within $9\Delta_{by}$.

Fig. 27. Spliced BRB installation.

the spliced BRB was comparable to a standard BRB and has repeatable and expected hysteretic behavior. In fact, the testing program carried out as part of this project showed that a properly designed and detailed BRB can withstand testing that is well in excess of the current AISC 341-10 testing protocol in terms of cumulative ductility and maximum ductility demand. A prototype test program was instrumental in assessing constructability, tolerances and other potential issues prior to actual construction. In addition, preconstruction planning and close coordination among the engineer, fabricator and contractor are crucial for a successful project.

Studies by Fahnestock et al. (2006), Mayes et al. (2004) and Sabelli et al. (2003) have indicated that the current protocol shown in AISC 341-10 cyclic testing for qualification of BRBs may not be adequate to capture maximum ductility demands on the BRBs, especially under maximum considered earthquakes

ACKNOWLEDGMENTS

The project team consisted of Simpson Gumpertz and Heger, BAGG Engineers and Eichleay Engineers. The BRB suppliers, CoreBrace Inc. and the National Center for Research on Earthquake Engineering (NCREE), Taiwan, provided generous assistance in this project. Their help is gratefully acknowledged. The opinions and findings are those of the authors and do not necessarily reflect the views of individuals acknowledged herein.

REFERENCES

AISC (2010), *Seismic Provisions for Structural Steel Buildings,* AISC 341-10, American Institute of Steel Construction, Chicago, IL.

ASCE (2006), *Seismic Rehabilitation of Existing Buildings,* ASCE-41-06, American Society of Civil Engineers, Reston, VA.

Fahnestock, A.L., Sause, R. and Ricles, J.M. (2006) "Analytical and Large-Scale Experimental Studies of Earthquake-Resistant Buckling Restrained Braced Frame Systems," ATLSS Report No. 06-01*,* September 2006.

Mayes, R.L., Goings, C., Wassim, H., Harris, S., Lovejoy, J, Fanucci, J. P., Bystricky, P. and Hayes, J.R. (2004) "Comparative Performance of Buckling-Restraint Braces and Moment Frames," *Proc. 13th World Conference on Earthquake Engineering*, Vancouver, BC, Canada, Paper No. 2887.

Sabelli R., Mahin, S. and Chang, C. (2003). "Seismic Demands on Steel Braced Frame Buildings with Buckling Restrained Braces," *Engineering Structures*, Vol. 25, No. 5, April, pp. 655–666.

Tsai, K.C., Wei, C.Y., Wu, A.C., Lin, T.H. and Chen, J.C. (2010a), *Subassemblage Testing of Corebrace Buckling-Restrained Braces Using Pin Connection*, Report No. NCREE-02/10-01, National Center for Research on Earthquake Engineering, Taiwan.

Tsai, K.C., Wei, C.Y., Wu, A.C., Lin, T.H. and Chen, J.C. (2010b), *Subassemblage Testing of Corebrace Buckling-Restrained Braces using Bolted Connection*, Report No. NCREE-02/10-02, National Center for Research on Earthquake Engineering, Taiwan.

Local Stability of Double-Coped Beams

BO DOWSWELL and ROBERT WHYTE

ABSTRACT

Localized web buckling can limit the strength of coped beams. In this paper, the coped portion of the beam is treated as an isolated rectangular member, and a parametric study is used to develop lateral-torsional buckling modification factors for use with 2010 AISC *Specification* Section F11. The parametric study included finite element models with different cope lengths at the top and bottom flanges and cope depths up to 40% of the beam depth. Compared with the finite element results in this paper, the proposed design procedure is more accurate than the design procedure in the 14th Edition *Steel Construction Manual*.

Keywords: web buckling, coped beams, double copes.

INTRODUCTION

In beam-to-girder connections, the beam is usually coped to allow a standard connection to the girder web. If the beam and girder are of equal nominal depth, both flanges must be coped as shown in Figure 1. The cope length can be large at skewed beam connections; connections to wide flange truss chords; and other, less-common framing conditions. Additionally, it is common for double-coped beams to have unequal cope depths at the top and the bottom, and some connections require unequal cope lengths.

Due to the flexural and shear stresses in the coped portion of the web, web buckling can limit the local strength. The AISC *Steel Construction Manual* (AISC, 2011) provides a design procedure for localized stability of double-coped beams. The equations were developed by Cheng, Yura and Johnson (1984) based on a lateral torsional buckling model with an adjustment factor determined by curve-fitting data from elastic finite element models. Because the adjustment factor was derived using finite element models, limits of applicability were placed on the design equations. One goal of this paper is to expand the finite element database and the limits of applicability of the design equations.

EXISTING PUBLICATIONS

Cheng et al. (1984)

Cheng et al. (1984) developed the design procedure in the AISC *Steel Construction Manual* (AISC, 2011) with the results of 14 elastic finite element models. BASP finite element software was used as described by Akay, Johnson and Will (1977). The models were braced laterally at the face of the compression flange cope. The buckled shapes showed that the tension edge of the coped cross-section experienced lateral movement, and the shear center of the coped region experienced lateral movement and twisting. The design procedure was developed based on a lateral torsional buckling model with an adjustment factor determined by curve-fitting data from the finite element models. All models had maximum cope depths of 20% of the beam depth and equal cope sizes at the top and bottom flanges.

Steel Construction Manual (AISC, 2011)

The model for the design procedure developed by Cheng et al. (1984) is shown in Figure 1. The required flexural strength at the face of the cope is

$$M_r = R_r e \tag{1}$$

The nominal flexural strength is

$$M_n = F_{cr} S_{net} \tag{2}$$

The critical stress is

$$F_{cr} = 0.62\pi E f_d \frac{t_w^2}{ch_0} \le F_y \tag{3}$$

The adjustment factor is

$$f_d = 3.5 - 7.5\left(\frac{d_{ct}}{d}\right) \tag{4}$$

where

E = modulus of elasticity, ksi
F_y = specified minimum yield stress, ksi
R_r = required end reaction, kips

Bo Dowswell, P.E., Ph.D., Principal, ARC International LLC, Birmingham, AL (corresponding). E-mail: bo@arcstructural.com

Robert Whyte, P.E., S.E., Assistant Project Manager, LBYD Inc., Birmingham, AL. E-mail: rwhyte@lbyd.com

S_{net} = section modulus of the coped section, in.^{3}
c = cope length, in.
d = beam depth, in.
d_{ct} = depth of the top cope, in.
e = distance from the face of the cope to the end reaction, in.
h_o = reduced depth of web, in.
t_w = web thickness, in.

The preceding equations are based on a lateral torsional buckling model and are valid when $c \le 2d$ and $d_c \le 0.2d$. If $d_c > 0.2d$, the following equations, which are based on a plate-buckling model (Muir and Thornton, 2004), are applicable.

$$F_{cr} = F_y Q \tag{5}$$

The reduction factor for plate buckling is

when $\lambda \le 0.7$

$$Q = 1.0 \tag{6a}$$

when $0.7 < \lambda \le 1.41$

$$Q = 1.34 - 0.486\lambda \tag{6b}$$

when $\lambda > 1.41$

$$Q = \frac{1.30}{\lambda^2} \tag{6c}$$

The slenderness parameter is

$$\lambda = \frac{h_0}{10t_w}\sqrt{\frac{F_y}{475 + 280\left(\frac{h_0}{c}\right)^2}} \tag{7}$$

Figure 2 shows a plot of the critical stress, F_{cr}, versus h_o/d for $c/d = 1$ and $t_w = 0.3$ in. The critical stress for lateral torsional buckling is calculated with Equations 3 and 4 without the yield stress limit. The critical stress for local buckling is calculated with Equations 5, 6 and 7. It can be seen that the two curves are trending in opposite directions, with F_{cr} increasing with h_o/d for lateral torsional buckling and decreasing with h_o/d for local buckling. This indicates the need for a single, continuous function that covers the entire range of applicability.

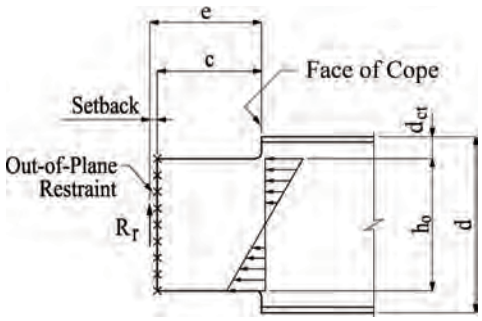

Fig. 1. Double-coped beam.

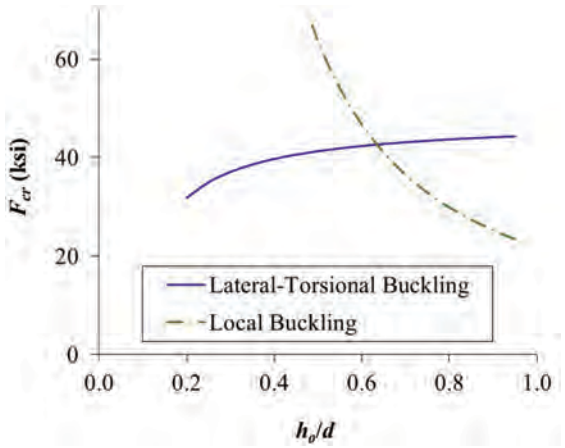

Fig. 2. Critical stress versus h_o/d.

AISC *Specification* Section F11

Because the *Manual* equations developed by Cheng et al. (1984) were based on a lateral torsional buckling model, AISC *Specification* (AISC, 2010) Section F11 will be reviewed here. Section F11 provides design information for the flexural strength and stability of rectangular members bent about their major axis.

For yielding, $\frac{L_b d}{t^2} \le \frac{0.08E}{F_y}$

$$M_n = M_p = F_y Z \le 1.6M_y \tag{8}$$

For inelastic lateral torsional buckling, $\frac{0.08E}{F_y} < \frac{L_b d}{t^2} \le \frac{1.9E}{F_y}$

$$M_n = C_b\left[1.52 - 0.274\left(\frac{L_b d}{t^2}\right)\frac{F_y}{E}\right]M_y \le M_p \tag{9}$$

For elastic lateral torsional buckling, $\frac{L_b d}{t^2} > \frac{1.9E}{F_y}$

$$M_n = F_{cr} S_x \le M_p \tag{10}$$

The critical stress is

$$F_{cr} = \frac{1.9EC_b}{\frac{L_b d}{t^2}} \tag{11}$$

where

C_b = lateral torsional buckling modification factor
L_b = distance between brace points, in.
M_n = nominal moment, kip-in.
M_y = yield moment, kip-in.
M_p = plastic moment, kip-in.
S_x = elastic section modulus, in.^{3}
Z = plastic modulus, in.^{3}
t = beam width, in.

Equation 11 is the theoretical solution for lateral torsional buckling (Timoshenko and Gere, 1961) multiplied by C_b and simplified by substituting the properties for a rectangular cross-section. It can be shown that Equation 3 is equal to Equation 11 by substituting $t = t_w$, $d = h_0$, $L_b = c$ and $C_b = f_d$ into Equation 11. Therefore, f_d is simply a lateral torsional buckling modification factor applied to the theoretical equation for the critical moment of a rectangular beam.

FINITE ELEMENT MODELS

AISC *Specification* Section F2 equations for lateral torsional buckling of wide flange beams are based on the theoretical solution (Timoshenko and Gere, 1961), with C_b factors developed primarily using elastic finite element models. The inelastic portion of the buckling curve was developed by mapping, based on limited testing and finite element results in the inelastic zone. Because much of the inelastic research was based on a constant moment along the beam length ($C_b = 1$), the full beam length was inelastic. Therefore, the buckling curves are conservative for $C_b > 1$ because they don't account for partial inelasticity along the beam. This same procedure was used in this research to develop equations for the local stability of coped beams.

The finite element program was designed to address three issues related to the local stability of double-coped beams:

1. Cope depths greater than 20% of the beam depth.
2. Unequal cope depths at the top and bottom.
3. Unequal cope lengths at the top and bottom.

A parametric study consisting of 54 elastic, finite element models was used to determine the effect of each variable on the critical load. Using the variables shown in Figure 3, the program consisted of 30 models with $c_t = c_b$, 12 models with $c_t > c_b$, and 12 models with $c_t < c_b$. The details are listed in Appendix A, Tables A1, A2 and A3, respectively.

All models were built with the nominal dimensions of a W16×26. Models for additional beam sizes are not required because the critical moment is proportional to t_w^3 for beams with identical proportions on the cope geometry. Following the modeling techniques of Cheng et al. (1984), BASP finite element software was used to determine the critical loads, assuming the flanges were laterally braced at the face of the cope. There was no setback dimension in the models; therefore, $c_t = e_t$ and $c_b = e_b$.

RESULTS

Accuracy of Manual Equations

For the models with equal cope lengths at the top and bottom flanges, Table A1 in Appendix A compares the finite element results to the current design procedure in the AISC *Manual* (AISC, 2011). Column 6 lists the critical reactions from the finite element models, R_{fe}, and column 7 lists the critical reactions from AISC *Manual* equations, R_{ce}. Models 1, 2, 5, 6, 11, 12, 15 and 16 had $d_c \le 0.2d$; therefore, R_{ce} was calculated with Equations 1 through 4. For the remaining specimens, R_{ce} was calculated with Equations 5, 6 and 7. The average R_{fe}/R_{ce} ratio, listed in column 10, is 1.54 with a standard deviation of 0.496.

Design Model

All of the finite element models buckled in a similar manner, as shown in Figure 4. Confirming the results of Cheng et al. (1984), the tension edge of the coped cross-section experienced lateral translation, and the shear center experienced lateral translation and twisting. The compression edge of the coped section buckled in the shape of a half sine wave, which extended partially into the uncoped portion of the beam due to lateral translation at the reentrant corner of the cope.

To form a design model, the buckling mode must be identified. The buckled shapes have the appearance of several independent modes, including local buckling, lateral torsional buckling, shear buckling, and distortional buckling.

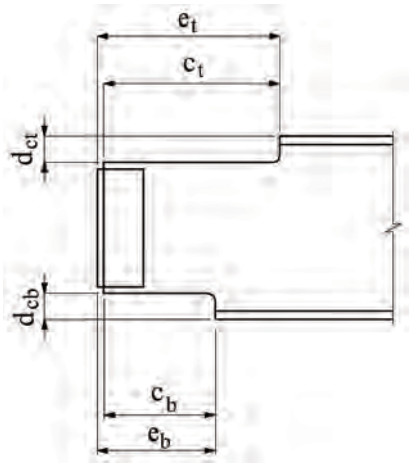

Fig. 3. Different cope sizes at the top and bottom flanges.

The dominant buckling mode is dependent on the cope geometry. Short copes are controlled by shear buckling, and long copes are controlled by lateral torsional buckling, with some aspects of local buckling and distortional buckling present in all cope geometries. Because the buckled shapes most closely resemble lateral torsional buckling over the critical variable range, the design model is based on Equation 11, with the buckling modification factor, C_b, accounting for contributions from the other buckling modes. Factor C_b was determined by curve-fitting the finite element data.

Curve-Fit Equations

The required flexural strength at the face of the cope is

$$M_r = R_r e_{min} \tag{12}$$

The nominal moment is calculated with Equations 10 and 11 with $t = t_w$ and $d = h_0$. The equation for C_b is dependent on the c_t/c_b ratio. For beams with $c_t = c_b$, C_b is calculated using Equation 13 with $L_b = c_t = c_b$. For beams with $c_t < c_b$, C_b is calculated using Equation 13 with $L_b = 0.9c_t + 0.1c_b$.

$$C_b = \left[3.3 + 0.85\sqrt{\frac{d}{L_b}}\ln\left(\frac{L_b}{d}\right)\right]\left[1 - \frac{d_{ct}}{d} + \left(\frac{d_{ct}}{d}\right)^2\right] \tag{13}$$

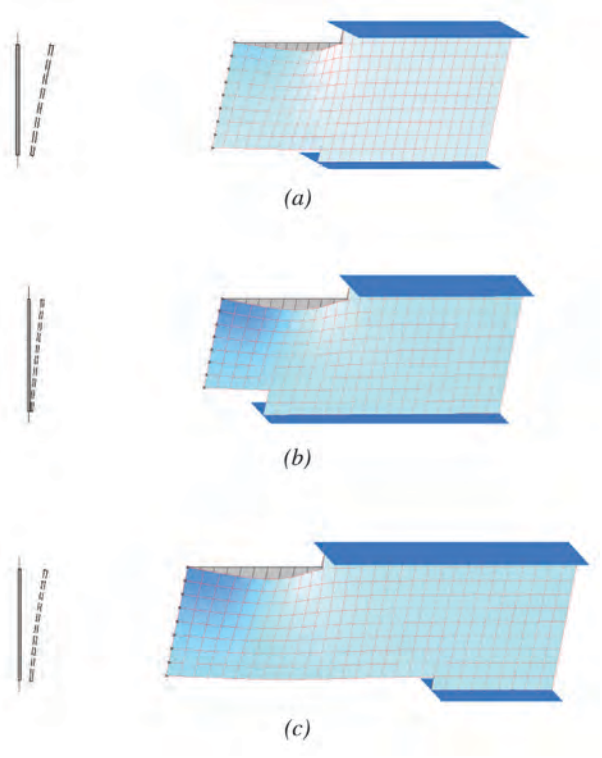

Fig. 4. Buckled shapes: (a) $c_t = c_b$; (b) $c_t > c_b$; (c) $c_t < c_b$.

For beams with $c_t > c_b$, C_b is calculated using Equation 14 with $L_b = (c_t + c_b)/2$.

$$C_b = \left(\frac{c_b}{c_t}\right)\left[3.3 + 0.85\sqrt{\frac{d}{L_b}}\ln\left(\frac{L_b}{d}\right)\right]\left[1 - \frac{d_{ct}}{d} + \left(\frac{d_{ct}}{d}\right)^2\right] \tag{14}$$

where

c_b = length of bottom cope, in.
c_t = length of top cope, in.
d_{cb} = depth of bottom cope, in.
d_{ct} = depth of top cope, in.
e_b = distance from the face of the bottom cope to the end reaction, in.
e_t = distance from the face of the top cope to the end reaction, in.
e_{min} = minimum of e_t and e_b

The results for all models are listed in Tables A1, A2 and A3 in Appendix A. For beams with $c_t = c_b$, the average, finite element-to-calculated load ratio is 1.01 and the standard deviation is 0.0535. For $c_t < c_b$, the average load ratio is 1.02, and the standard deviation is 0.0902. For $c_t > c_b$, the average load ratio is 1.06, and the standard deviation is 0.0752.

Equation 13 is plotted in Figures 5 and 6 with the finite element results for $c_t = c_b$. Figure 5 shows C_b versus c_t/d for four values of d_{ct}/d. Figure 6 shows C_b versus d_{ct}/d for four values of c_t/d.

DESIGN

Moment-Shear Interaction

The design procedure in the AISC *Manual* (AISC, 2011) uses beam theory as the basis for calculation of the flexural stresses. Because the maximum normal and shear stresses occur at different locations on the cross-section, combining these stresses is not required. However, the design procedure proposed in this paper utilizes the plastic flexural strength. Because the plastic stress distribution requires the maximum shear and normal stresses to act at the same location on the cross-section, the flexural strength is reduced in the presence of shear loading. For short cope lengths, the required shear load can be close to the shear yield strength. To account for the interaction between the flexural and shear loads, a reduction factor can be applied to the plastic moment capacity, M_p. Neal (1961) developed Equation 15 for the plastic capacity of a rectangular member subjected to moment about one axis, axial load and shear.

$$\frac{M_r}{M_p} + \left(\frac{P_r}{P_y}\right)^2 + \frac{\left(\frac{R_r}{V_n}\right)^4}{1 - \left(\frac{P_r}{P_y}\right)^2} \le 1.0 \tag{15}$$

where

P_r = required axial load, kips
P_y = axial yield load, kips
R_r = required shear load, kips
V_n = shear yield strength, = $0.6F_y h_o t_w$, kips

The plastic moment strength, reduced to account for the required shear load is

$$M_{pv} = M_p \left[1 - \left(\frac{R_r}{V_n} \right)^4 \right] \tag{16}$$

Because M_{pv} must be based on the available shear strength rather than the nominal value, Equations 17a and 17b should be used in design:

$$\text{LRFD} \qquad M_{pv} = M_p \left[1 - \left(\frac{R_r}{\phi_v V_n} \right)^4 \right] \tag{17a}$$

$$\text{ASD} \qquad M_{pv} = M_p \left[1 - \left(\frac{\Omega_v R_r}{V_n} \right)^4 \right] \tag{17b}$$

Limits of Applicability

Because the curve-fit equations were derived using finite element models, the range of applicability should be based on the cope geometries studied. The geometry of the tension flange cope has a limited influence on the buckling load; therefore, no limits are required on d_{cb} or c_b. The finite element models were limited to a maximum cope length of

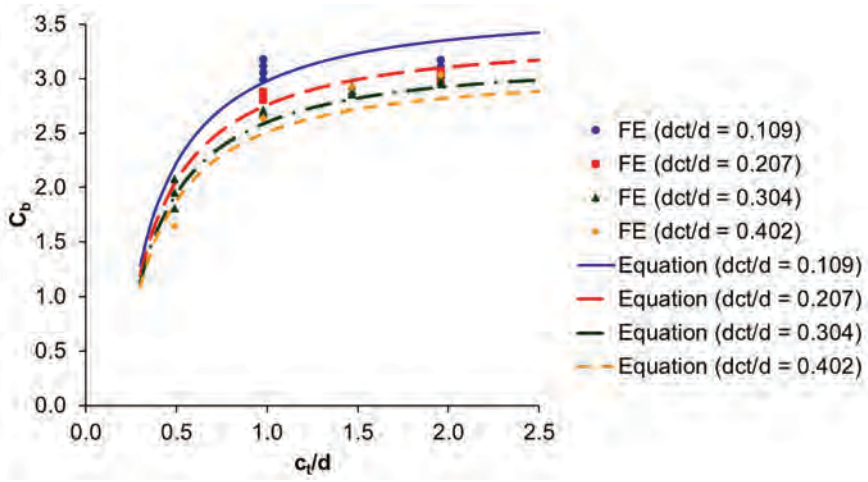

Fig. 5. C_b *versus* c_t/d.

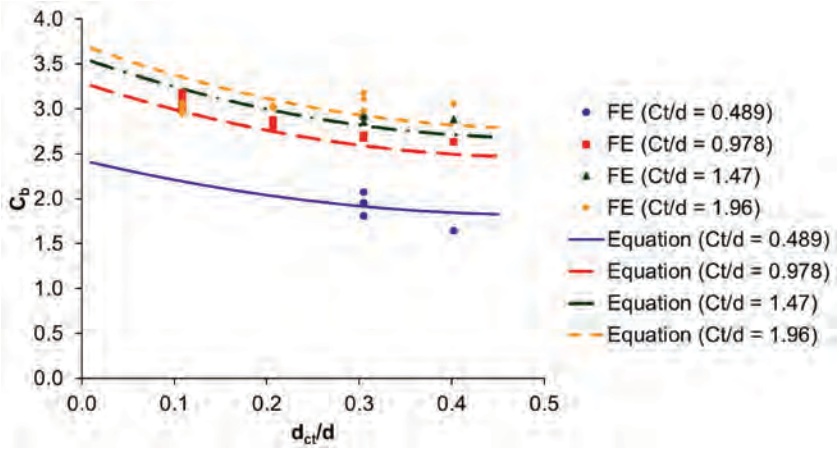

Fig. 6. C_b *versus* d_{ct}/d.

twice the beam depth. Observation of Figure 5 shows that C_b increases slowly for c_t/d greater than 2; therefore, in the rare case that $c_t > 2d$, it is recommended that $c_t = 2d$ is used in the calculations. Because the depth of the compression flange cope was limited to 40% of the beam depth, the equations are valid only for $d_{ct} \le 0.4d$.

When c_t/d is less than 0.5, the curve-fit equations can produce unrealistically low values for C_b. This is because shear buckling dominates the behavior for short copes. To eliminate erroneous calculations, a lower limit can be applied to C_b. According to equations developed by Dowswell (2004), C_b = 1.84 for a rectangular cantilever beam loaded at the shear center with bracing at each end and a concentrated load at the tip. Therefore, a minimum value of C_b = 1.84 is recommended.

Design Proposal

To account for inelastic action, AISC *Specification* Section F11 can be used with $t = t_w$ and $d = h_0$. The following design procedure is suggested:

For yielding, $\lambda \le \lambda_p$:

$$M_n = M_{pv} \tag{18}$$

For inelastic lateral-torsional buckling, $\lambda_p < \lambda \le \lambda_r$:

$$M_n = C_b\left[1.52 - 0.274\lambda\frac{F_y}{E}\right]M_y \le M_{pv} \tag{19}$$

For elastic lateral-torsional buckling, $\lambda > \lambda_r$:

$$M_n = F_{cr}S_x \le M_{pv} \tag{20}$$

The critical stress is

$$F_{cr} = \frac{1.9EC_b}{\lambda} \tag{21}$$

where

$$\lambda = \frac{L_b h_0}{t_w^2} \tag{22}$$

$$\lambda_p = \frac{0.08E}{F_y} \tag{23}$$

$$\lambda_r = \frac{1.9E}{F_y} \tag{24}$$

Simplified Equations

Simplified versions of Equations 13 and 14 can be used for design purposes. For beams with $c_t = c_b$ and beams with $c_t < c_b$, $L_b = c_t$ and C_b is calculated with Equation 25.

$$C_b = \left[3 + \ln\left(\frac{L_b}{d}\right)\right]\left(1 - \frac{d_{ct}}{d}\right) \le 1.84 \tag{25}$$

For beams with $c_t > c_b$, $L_b = (c_t + c_b)/2$ and C_b is calculated with Equation 26.

$$C_b = \left(\frac{c_b}{c_t}\right)\left[3 + \ln\left(\frac{L_b}{d}\right)\right]\left(1 - \frac{d_{ct}}{d}\right) \le 1.84 \tag{26}$$

The simplified equations are compared with the finite element models in Appendix A, Tables A1, A2 and A3. For beams with $c_t = c_b$, the average finite element-to-calculated load ratio is 1.18, and the standard deviation is 0.139. For $c_t < c_b$, the average load ratio is 1.05, and the standard deviation is 0.0736. For $c_t > c_b$, the average load ratio is 1.19, and the standard deviation is 0.0949.

CONCLUSIONS

This paper used the results of a parametric study to formulate a design procedure for the local strength of double-coped beams. Lateral torsional buckling modification factors, for use with AISC *Specification* Section F11, were formulated by curve-fitting the results of 54 finite element models. The proposed solution is based on a larger database of finite element models than the *Manual* procedure, and the limits of applicability have been extended. In contrast to the *Manual* procedure, which has curves trending in opposite directions, the proposed solution provides a single, continuous equation over the entire range of applicability.

The proposed design procedure was shown to be more accurate than the current *Manual* procedure. For beams with equal cope lengths at both flanges, the *Manual* procedure has an average finite element–to–calculated load ratio of 1.54 with a standard deviation of 0.496. The curve-fit equation developed in this paper (Equation 13) produced an average finite element–to–calculated load ratio of 1.01 with a standard deviation of 0.0535. For the simplified equation (Equation 25), the average finite element–to–calculated load ratio is 1.18 with a standard deviation of 0.139.

Using all 54 of the finite element results, calculations using the curve-fit equations (Equations 13 and 14) produced an average finite element–to–calculated load ratio of 1.02 and a standard deviation of 0.0665. The simplified design equations (Equations 25 and 26) had an average finite element–to–calculated load ratio of 1.15 and a standard deviation of 0.115.

ACKNOWLEDGMENTS

The authors would like to thank Professor Joseph Yura at the University of Texas at Austin for providing the finite element program, BASP, used in this study.

SYMBOLS

C_b = lateral torsional buckling modification factor

E = modulus of elasticity, ksi

F_{cr} = critical stress, ksi

F_y = specified minimum yield stress, ksi

L_b = distance between brace points, in.

M_n = nominal moment, kip-in.

M_y = yield moment, kip-in.

M_p = plastic moment, kip-in.

M_{pv} = plastic moment, reduced to account for the required shear load, kip-in.

M_r = required moment, kip-in.

P_r = required axial load, kips

P_y = axial yield load, kips

Q = reduction factor for plate buckling

R_{de} = critical reaction with C_b calculated with the simplified design equation

R_{fe} = critical reaction from finite element model

R_r = required end reaction, kips

R_{re} = critical reaction with C_b calculated with the original regression equation

S_{net} = elastic section modulus of the coped section, in.^{3}

S_x = elastic section modulus, in.^{3}

V_n = shear yield strength, kips

Z = plastic modulus, in.^{3}

c = cope length, in.

c_b = length of bottom cope, in.

c_t = length of top cope, in.

d = beam depth, in.

d_{cb} = depth of bottom cope, in.

d_{ct} = depth of top cope, in.

e = distance from the face of the cope to the end reaction, in.

e_b = distance from the face of the bottom cope to the end reaction, in.

e_t = distance from the face of the top cope to the end reaction, in.

e_{min} = minimum of e_t and e_b

f_d = adjustment factor

h_o = reduced depth of web, in.

t = beam width, in.

t_w = web thickness, in.

Ω_v = safety factor for shear

ϕ_v = resistance factor for shear

λ = slenderness parameter

λ_p = limiting slenderness for the limit state of yielding

λ_r = limiting slenderness for the limit state of inelastic lateral torsional buckling

REFERENCES

AISC (2010), *Specification for Structural Steel Buildings*, American Institute of Steel Construction, Chicago, IL.

AISC (2011), *Steel Construction Manua*l, 14th ed., American Institute of Steel Construction, Chicago, IL.

Akay, H.U., Johnson, C.P. and Will, K.M. (1977), "Lateral and Local Buckling of Beams and Frames," *Journal of the Structural Division,* ASCE, Vol. 103, No. ST9, September, pp. 1821–1832.

Cheng, J.J., Yura, J.A. and Johnson, C.P. (1984), "Design and Behavior of Coped Beam," Ferguson Lab Report, The University of Texas at Austin, July.

Dowswell, B. (2004), "Lateral-Torsional Buckling of Wide Flange Cantilever Beams," *Engineering Journal*, AISC, Second Quarter, Vol. 41, No. 2.

Muir, L.S. and Thornton, W.A. (2004), "A Direct Method for Obtaining the Plate Buckling Coefficient for Double-Coped Beams," *Engineering Journal*, AISC, Third Quarter, Chicago, IL.

Neal, B.G. (1961), "The Effect of Shear and Normal Forces on the Fully Plastic Moment of a Beam of Rectangular Cross Section," *Journal of Applied Mechanics,* Vol. 28, pp. 269–274.

Timoshenko, S. P. and Gere, J. M. (1961), *Theory of Elastic Stability*, 2nd ed., McGraw-Hill, New York.

APPENDIX A. TABLES

Table A1. Finite Element Results with $c_t = c_b$

Model Number	c_t (in.)	c_b (in.)	d_{ct} (in.)	d_{cb} (in.)	R_{fe} (kips)	R_{ce} (kips)	R_{re} (kips)	R_{de} (kips)	$\frac{R_{fe}}{R_{ce}}$	$\frac{R_{fe}}{R_{re}}$	$\frac{R_{fe}}{R_{de}}$
1	15.4	15.4	1.71	1.71	24.4	20.6	22.7	20.3	1.18	1.07	1.20
2	15.4	15.4	3.24	1.71	19.3	13.1	18.4	15.8	1.48	1.05	1.22
3	15.4	15.4	4.78	1.71	15.6	9.35	14.9	11.9	1.66	1.05	1.31
4	15.4	15.4	6.31	1.71	12.6	7.10	11.9	8.53	1.78	1.06	1.48
5	15.4	15.4	1.71	3.24	20.9	18.0	19.9	17.8	1.16	1.05	1.18
6	15.4	15.4	3.24	3.24	16.3	11.2	15.8	13.6	1.46	1.04	1.20
7	15.4	15.4	4.78	3.24	12.9	7.10	12.4	9.92	1.82	1.04	1.30
8	15.4	15.4	1.71	4.78	17.6	9.35	17.0	15.3	1.88	1.03	1.15
9	15.4	15.4	3.24	4.78	13.4	7.10	13.1	11.3	1.89	1.02	1.19
10	15.4	15.4	1.71	6.31	14.3	7.10	14.2	12.7	2.02	1.01	1.13
11	30.7	30.7	1.71	1.71	6.09	5.14	6.42	6.27	1.18	0.948	0.970
12	30.7	30.7	3.24	1.71	5.16	3.27	5.20	4.88	1.58	0.992	1.06
13	30.7	30.7	4.78	1.71	4.36	4.45	4.20	3.67	0.979	1.04	1.19
14	30.7	30.7	6.31	1.71	3.63	3.46	3.37	2.63	1.05	1.08	1.38
15	30.7	30.7	1.71	3.24	5.22	4.50	5.62	5.49	1.16	0.930	0.951
16	30.7	30.7	3.24	3.24	4.34	2.80	4.46	4.19	1.55	0.973	1.04
17	30.7	30.7	4.78	3.24	3.57	3.46	3.50	3.06	1.03	1.02	1.17
18	30.7	30.7	1.71	4.78	4.41	4.45	4.81	4.70	0.989	0.915	0.937
19	30.7	30.7	3.24	4.78	3.57	3.46	3.71	3.49	1.03	0.961	1.02
20	30.7	30.7	1.71	6.31	3.63	3.46	4.01	3.92	1.05	0.906	0.927
21	7.68	7.68	4.78	1.71	41.6	21.0	44.1	36.6	1.98	0.945	1.14
22	7.68	7.68	6.31	1.71	31.5	15.3	35.4	26.2	2.06	0.891	1.20
23	7.68	7.68	4.78	3.24	37.4	15.3	36.7	30.5	2.45	1.02	1.23
24	23.0	23.0	4.78	1.71	7.51	6.02	7.19	6.01	1.25	1.04	1.25
25	23.0	23.0	6.31	1.71	6.22	4.64	5.77	4.31	1.34	1.08	1.44
26	23.0	23.0	4.78	3.24	6.15	4.64	5.99	5.01	1.32	1.03	1.23
27	7.68	7.68	4.78	4.78	31.8	10.2	29.4	24.4	3.11	1.08	1.31
28	15.4	15.4	4.78	4.78	10.3	4.96	9.91	7.94	2.07	1.04	1.29
29	23.0	23.0	4.78	4.78	4.87	3.28	4.79	4.01	1.49	1.02	1.21
30	30.7	30.7	4.78	4.78	2.83	2.45	2.80	2.45	1.15	1.01	1.16
								Average	1.54	1.01	1.18
								Standard Deviation	0.496	0.0535	0.139

R_{fe} = critical reaction from finite element model
R_{ce} = critical reaction from AISC *Manual* equations
R_{re} = critical reaction with C_b calculated with the original regression equation
R_{de} = critical reaction with C_b calculated with the simplified design equation

Table A2. Finite Element Results with $c_t > c_b$									
Model Number	**c_t (in.)**	**c_b (in.)**	**d_{ct} (in.)**	**d_{cb} (in.)**	**R_{fe} (kips)**	**R_{re} (kips)**	**R_{de} (kips)**	**$\frac{R_{fe}}{R_{re}}$**	**$\frac{R_{fe}}{R_{de}}$**
32	30.7	15.4	3.24	3.24	6.87	5.72	5.14	1.20	1.33
34	30.7	15.4	1.71	1.71	8.27	8.24	7.71	1.00	1.07
36	30.7	15.4	1.71	3.24	7.69	7.21	6.74	1.07	1.14
38	30.7	15.4	3.24	1.71	7.41	6.67	6.00	1.11	1.23
40	15.4	7.68	3.24	3.24	20.5	19.2	16.4	1.07	1.25
42	15.4	7.68	1.71	1.71	27.9	27.6	24.5	1.01	1.14
44	15.4	7.68	1.71	3.24	25.7	24.2	21.4	1.06	1.20
46	15.4	7.68	3.24	1.71	22.3	22.4	19.1	0.995	1.17
48	30.7	7.68	3.24	3.24	7.94	6.64	5.84	1.19	1.36
50	30.7	7.68	1.71	1.71	9.10	9.57	8.75	0.952	1.04
52	30.7	7.68	1.71	3.24	8.79	8.37	7.65	1.05	1.15
54	30.7	7.68	3.24	1.71	8.25	7.75	6.81	1.06	1.21
							Average	1.06	1.19
							Standard Deviation	0.0752	0.0949

R_{fe} = critical reaction from finite element model
R_{re} = critical reaction with C_b calculated with the original regression equation
R_{de} = critical reaction with C_b calculated with the simplified design equation

Table A3. Finite Element Results with $c_t < c_b$									
Model Number	**c_t (in.)**	**c_b (in.)**	**d_{ct} (in.)**	**d_{cb} (in.)**	**R_{fe} (kips)**	**R_{re} (kips)**	**R_{de} (kips)**	**$\frac{R_{fe}}{R_{re}}$**	**$\frac{R_{fe}}{R_{de}}$**
31	15.4	30.7	3.24	3.24	14.1	14.7	13.6	0.959	1.04
33	15.4	30.7	1.71	1.71	21.3	21.1	20.3	1.01	1.05
35	15.4	30.7	1.71	3.24	18.5	18.5	17.8	1.00	1.04
37	15.4	30.7	3.24	1.71	16.5	17.1	15.8	0.962	1.04
39	7.68	15.4	3.24	3.24	42.8	45.1	41.7	0.948	1.03
41	7.68	15.4	1.71	1.71	72.6	65.0	62.4	1.12	1.16
43	7.68	15.4	1.71	3.24	64.4	56.9	54.6	1.13	1.18
45	7.68	15.4	3.24	1.71	48.7	52.6	48.6	0.926	1.00
47	7.68	30.7	3.24	3.24	40.3	41.7	41.7	0.967	0.967
49	7.68	30.7	1.71	1.71	68.3	60.0	62.4	1.14	1.09
51	7.68	30.7	1.71	3.24	61.3	52.5	54.6	1.17	1.12
53	7.68	30.7	3.24	1.71	45.5	48.6	48.6	0.936	0.936
							Average	1.02	1.05
							Standard Deviation	0.0902	0.0736

R_{fe} = critical reaction from finite element model
R_{re} = critical reaction with C_b calculated with the original regression equation
R_{de} = critical reaction with C_b calculated with the simplified design equation

ERRATA

The Behavior of Steel Perimeter Columns in a High-Rise Building under Fire

Paper by MARIA M. GARLOCK and SPENCER E. QUIEL

(4th Quarter, 2007)

Figure 11 should be replaced with the following figure.

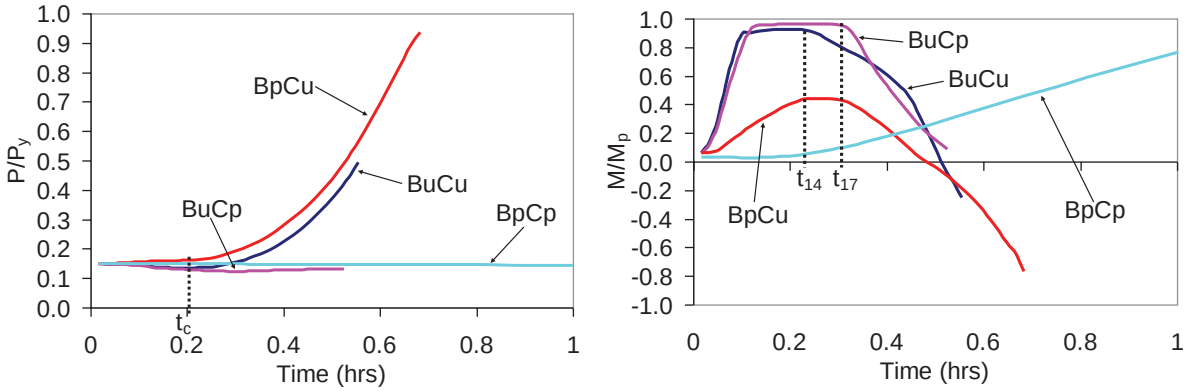

Fig. 11. Computational (SAFIR) results for (a) axial load ratio and (b) plastic moment ratio for the column just below Floor 23.

ERRATA

Flange Bending in Single Curvature*

Paper by BO DOWSWELL

(2nd Quarter, 2013)

Equations 33 and 38 should be replaced with the following:

$$C_{z1} = 1.81 - 1.15\lambda + 1.06e^{-7.70\lambda} \quad (33)$$

$$C_{z1} = 2.23 - 1.49\lambda + 1.39e^{-18.3\lambda} \quad (38)$$

*Another errata for this paper appears in 3rd Quarter 2013.

Guide for Authors

SCOPE: The ENGINEERING JOURNAL is dedicated to the improvement and advancement of steel construction. Its pages are open to all who wish to report on new developments or techniques in steel design, research, the design and/or construction of new projects, steel fabrication methods, or new products of significance to the uses of steel in construction. Only original papers should be submitted.

GENERAL: Papers intended for publication may be submitted by mail to the Editor, Keith Grubb, ENGINEERING JOURNAL, AMERICAN INSTITUTE OF STEEL CONSTRUCTION, One East Wacker Drive, Suite 700, Chicago, IL, 60601, or by email to grubb@aisc.org.

The articles published in the *Engineering Journal* undergo peer review before publication for (1) originality of contribution; (2) technical value to the steel construction community; (3) proper credit to others working in the same area; (4) prior publication of the material; and (5) justification of the conclusion based on the report.

All papers within the scope outlined above will be reviewed by engineers selected from among AISC, industry, design firms, and universities. The standard review process includes outside review by an average of three reviewers, who are experts in their respective technical area, and volunteers in the program. Papers not accepted will not be returned to the author. Published papers become the property of the American Institute of Steel Construction and are protected by appropriate copyrights. No proofs will be sent to authors. Each author receives three copies of the issue in which his contribution appears.

MANUSCRIPT PREPARATION: Manuscripts must be provided in Microsoft Word format. Include a PDF with your submittal. View our complete author guidelines at **www.aisc.org/ej**.

There's always a solution in steel.

ENGINEERING JOURNAL
American Institute of Steel Construction
One East Wacker Drive, Suite 700
Chicago, IL 60601

312.670.2400 www.aisc.org